12

Low-Temperature Thermometry

A thermometer is a device by which we can measure a property of matter which is connected via a physical law to the concept of "temperature", where the latter is defined by thermodynamics. Therefore knowledge about the obtained temperature depends both on the quality of the measurement and on the theory on which this physical law is based. In general, thermometers can be divided into two groups.

For *primary thermometers* our theoretical knowledge about the measured property of matter is good enough to calculate the thermodynamic temperature from it without any calibration. Examples of primary thermometers are gas thermometers (using the relation between pressure, volume and temperature for gases) (Sect. 12.1), measurements of the velocity of sound in a gas [$v = (\kappa\rho)^{-1/2}$], the Coulomb blockade of electrons in tunnel junctions (see Sect. 12.6), thermal noise of an electrical resistor (using the Nyquist equation, see Sect. 12.7), and the angular anisotropy of gamma rays emitted from radioactive nuclei (using the Boltzmann population of the various hyperfine levels, see Sect. 12.11). Usually primary thermometry is difficult and mostly left to specialized national standards laboratories. Therefore the *secondary thermometers* are the "workhorses" of thermometry in research laboratories. For these thermometers, theory is not at a stage such that we can calculate the temperature directly from the measured property. Secondary thermometers have to be calibrated with a primary thermometer and/or at fixed points, as discussed in Chap. 11. Secondary thermometers are often much more sensitive than primary thermometers, and usually they are much more convenient to use. Examples will be discussed in this chapter.

There are various requirements which a useful thermometer has to fulfil:

- The thermometer should have a wide operating temperature range and should be insensitive to environmental changes, such as magnetic fields
- The property x to be measured must be easily, quickly, reproducibly, and exactly accessible to an experiment

F. Pobell, *Matter and Methods at Low Temperatures*

- The temperature dependence of the measured property, $x(T)$, should be expressible by a reasonably simple law
- The sensitivity $(\Delta x/x)/(\Delta T/T)$ should be high
- The thermometer should reach equilibrium in a "short" time, both within itself and with its surroundings whose temperature it is supposed to measure. Therefore it should have a small heat capacity, good thermal conductivity and good thermal contact to its surroundings. In particular, the thermal contact problem is ever present for thermometry at $T \leq 1\,\mathrm{K}$.
- The relevant measurement should introduce a minimum of heat to avoid heating of the surroundings of the thermometer and, of course, above all, heating of itself; this becomes more important the lower the temperature.

There are many possible choices for a thermometer, and one of the first considerations has to be to select the one most appropriate for a particular experiment and temperature range. The recent achievements in refrigeration have required corresponding progress in thermometry. The substantial advancements in this field are reflected by the enormous number of papers on low-temperature thermometry published in journals such as the *Journal of Low Temperature Physics, Review of Scientific Instruments* and *Cryogenics*. It is impossible to give sufficient credit to all this work. Additional information can be found in [12.1–12.11].

The oldest methods of thermometry use thermometers based on the expansion of gases, liquids or solids when the temperature is changed. I discuss one of them here in Sect. 12.1 of this chapter.

12.1 Gas Thermometry

The gas thermometer [12.1, 12.2, 12.8–12.11, 12.14], in principle, is a primary thermometer based on the relation for an ideal gas

$$PV = nRT\,, \tag{12.1}$$

assuming that there are no interactions between the gas molecules and that their own volume is negligible. Real gases, of course, deviate from the behavior of an ideal gas, and therefore corrections to this equation ("virial coefficients") have to be applied. The measurement can be performed with a fixed amount of gas either at constant pressure or at constant volume. Figure 12.1 schematically illustrates the setups for these two procedures.

One of the requirements for gas thermometry is that the dead volumes (valves, tubes, manometers) are small and hopefully constant, because one has to correct for them. In addition, the thermal and elastic volume changes of the various components, and absorption and desorption of gas from the container walls have to be taken into account and, last but not least, the deviations from the ideal gas behavior, which are particularly important at low temperatures, must be known. In general, high-precision gas thermometry

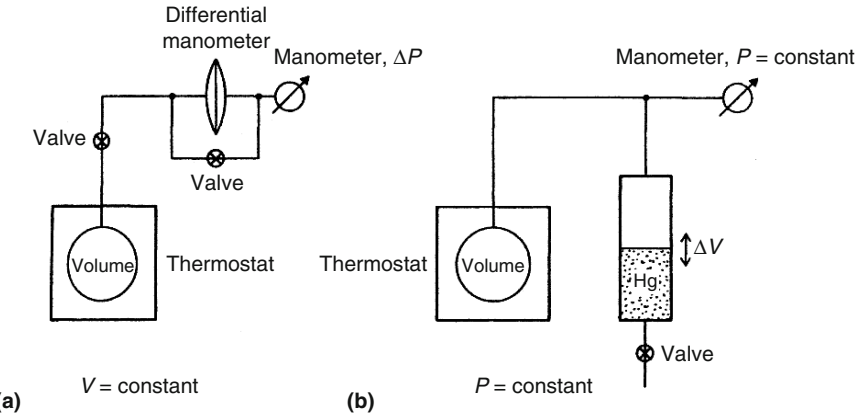

Fig. 12.1. Schematic setups for gas thermometry at (**a**) **V** = const. and (**b**) **P** = const.

is very tedious and therefore the gas thermometer is mostly used by national laboratories for calibration purposes or to establish the temperature scale. As discussed in Sect. 11.2, it is one of the devices used to establish the ITS-90, and that is the main reason for mentioning it here.

Other versions of gas thermometers are the acoustic gas thermometer (using the relation for the velocity of sound $v_s = (RTC_P/C_V M)^{1/2}$) or the dielectric constant thermometer (using the relation for the dielectric constant $\varepsilon = \varepsilon_0 + \alpha_0\ \mathrm{n\,V^{-1}}$, with ε_0 the exactly known dielectric constant and α_0 the static electric dipole polarizability of atoms). Again, these are the equations for the ideal gas, which have to be corrected by virial expansions for real gases [12.10].

12.2 Helium Vapour Pressure Thermometry

Another method relying on the behavior of the gas phase and on the Clausius–Clapeyron equation (2.8) is the determination of temperature by measurement of the vapour pressure above a cryogenic liquid. It is less complicated and more accurate than gas thermometry because the vapour pressure depends strongly on the temperature, see (2.10). Here one has to use the liquid which is appropriate for the relevant temperature range. Vapour pressure data for H_2, Ne, N_2 and O_2 can be found in [12.1], but, of course, the temperatures there have to be converted to the new ITS-90 scale (Sect. 11.2). Most frequently used for low-temperature physics is the measurement of the vapour pressure of the liquid helium isotopes which defines the ITS-90 scale from 0.65 to 5.0 K (Sects. 2.3.2 and 11.2). Helium vapour pressure thermometry is of particular importance for the calibration of resistance thermometers in the range from 0.5 to 4.2 K (Sect. 12.5). A vapour pressure thermometer has to be calibrated.

It is a secondary thermometer because our theoretical knowledge about the temperature dependence of the vapour pressure is not such that we can write down a complete and simple equation for it from first principles. The equation that we derived in Sect. 2.3.2 was a very rough approximation, assuming ideal gas behavior for the vapour and assuming the latent heat of evaporation to be temperature independent. Fortunately, calibration of the helium vapour pressure has been done very carefully by various laboratories in recent years to establish the ITS-90, where the P-T relations for the helium isotopes are given (Sect. 11.2). The new P-T values for the ^{3}He and ^{4}He vapour pressures calculated with (11.6) and with the coefficients given in Table 11.2, are listed in Tables 11.3 and 11.4.

To perform vapour pressure thermometry one needs data relating vapour pressure to temperature as well as a sensitive, calibrated manometer, and one has to minimize experimental errors [12.14]. Usually it is not sufficient just to measure the vapour pressure above the boiling cryoliquid because liquids have a low thermal conductivity (except superfluid helium), and therefore substantial temperature gradients may develop within them. For example, liquid ^{3}He at SVP shows a pronounced maximum in its density at 0.5 K. This anomaly and the low thermal conductivity of liquid ^{3}He (Figs. 2.17 and 2.18) at those temperatures can lead to a severe temperature (density) gradient in ^{3}He baths at $T < 0.5$ K, with the coldest part at the bottom, because in this case gravitationally driven convection does not occur. As a result, the temperature at the top of the liquid which determines the vapour pressure may be substantially different from the temperature lower down in the bath where the experiment is situated. The problem can be reduced by using only a thin layer of ^{3}He and well-conducting container walls. These problems are absent when superfluid ^{4}He with its very large thermal conductivity is used, but here problems may arise from the superfluid helium film (Sect. 2.3.5) creeping to warmer parts of the apparatus, where it evaporates. Also, one should never use the pumping tube to connect the cryogenic liquid to the manometer, because there is usually a pressure gradient along it. The connecting capillary should also not be connected to a point at a temperature lower than the one to be measured because here part of the vapour would recondense. This problem can be eliminated by using a vacuum jacket around the capillary. Figure 12.2 shows an improved method of vapour pressure thermometry using the vapour above the liquid in a small cell connected to the experimental whose temperature should be determined. Even doing it in this way may introduce errors if the capillary – connecting the vapour pressure bulb at low temperatures with the manometer at room temperatures – has a small diameter and if the vapour pressure is low. A so-called "thermomolecular pressure difference" between the low-temperature bulb and the room-temperature manometer will develop when the mean free path λ of the gas particles becomes comparable to the radius r of the connecting capillary [12.4, 12.12–12.14]. The equation for this difference is

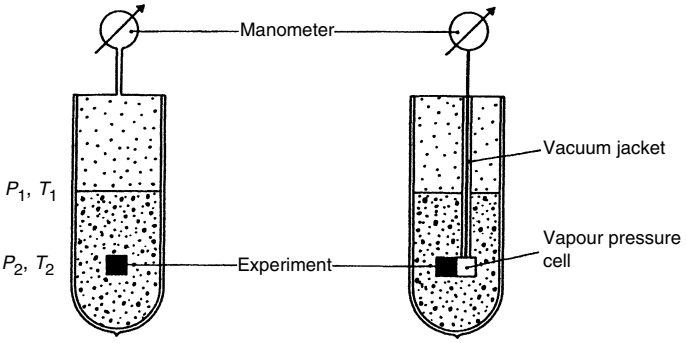

Fig. 12.2. Schematic setups for vapour pressure thermometry. *Left*: The vapour pressure above an evaporating cryoliquid is measured. Substantial temperature differences between the top of the liquid and the experiment can result due to the hydrostatic pressure head and temperature gradients in the liquid, which is usually not a good conductor (except for superfluid helium). *Right*: A small vapour pressure cell is connected to the experiment to avoid these problems. The capillary from this cell to the manometer at room temperature is vacuum jacketed to avoid changes due to a change in height of the cryoliquid

Table 12.1. Thermomolecular pressure correction for ^{3}He in a tube of radius r and with $T_{\rm warm} = 300\,{\rm K}$ and $T_{\rm cold} = 2\,{\rm K}$ at its ends [12.4, 12.12, 12.13]

$rP_{\rm warm}$ (mm mbar)	0.1	0.3	0.7	1.5	4
$P_{\rm cold}/P_{\rm warm}$	0.59	0.82	0.92	0.97	0.995

$$\frac{{\rm d}P}{{\rm d}T} = \frac{P}{2T} f(r/\lambda)\,, \tag{12.2}$$

where f is a function of the ratio r/λ. Table 12.1 lists some values for this correction for ^{3}He vapour with $T_{\rm cold} = 2\,{\rm K}$ and $T_{\rm warm} = 300\,{\rm K}$. The equation for the vapor pressure – if measured at room temperature – is then given by

$$P = P_{\rm measured} + \quad \Delta P_{\rm hydrost} + \Delta P_{\rm therm.mol.} \tag{12.3}$$

All these problems can be avoided if the pressure is measured not with a manometer at room temperature but with a cold manometer connected in situ directly to the refrigerated experiment. This low-temperature manometric vapour pressure thermometry can be done with very high precision with capacitive manometers, which will be discussed in Sect. 13.1. A capacitive vapour pressure thermometer with a resolution of about 10^{-9} over the limited temperature range $1.6\,{\rm K} \le T \le 2.2\,{\rm K}$ that uses a low temperature capacitive pressure transducer has been described in [12.15]. The design is similar to the earlier one of Greywall and Busch [12.16] to be discussed in Sect. 13.1, which has been used for vapour pressure thermometry below 1 K, but the new design

has a better long-term stability and resolution. Of course, it is only possible to take advantage of such a high-sensitivity thermometric device when an adequately designed stable thermal environment is available. This can be obtained by shielding the experiment with one or more temperature-regulated platforms or shields to which it is weakly thermally coupled [12.17].

The vapor pressure equations for liquid e-H_2, Ne, O_2, Ar, CH_4, CO_2, and for solid Ne, N_2, Ar and CO_2, in terms of the ITS-90 scale can be found in [12.1, 12.18].

12.3 Helium Melting Pressure Thermometry

The physics of liquid and solid ^{3}He determining the shape of its melting curve has already been discussed in Chap. 8; the melting curve is described by the Clausius–Clapeyron equation (8.2). The melting pressure of ^{3}He exhibits a pronounced temperature dependence (Fig. 8.1), which has been used as a rather precise thermometric standard, in particularly to establish the new temperature scale PLTS-2000 [12.19] (see Sect. 11.4) in the temperature range $0.9\,\mathrm{mK} < T < 1.0\,\mathrm{K}$ [12.19–12.24]. In addition, as also discussed in Sect. 11.3, the temperature of the minimum of the melting curve, the superfluid transitions of liquid ^{3}He, and the nuclear antiferromagnetic ordering transition of solid ^{3}He on the melting curve provide well-defined temperature fixed points independent of the pressure measurement, which can easily be detected using a melting curve thermometer. Alternatively, the pressures at which these transitions occur (Table 11.5) can be used to check the pressure calibration.

As a result of the earlier considerations, several groups investigating the properties of ^{3}He along the melting curve have used the melting pressure for thermometry at $T < 0.3\,\mathrm{K}$ in a similar way as helium vapour pressure is used for thermometry at higher temperatures. The pressure is measured as a function of temperature in situ capacitively with a capacitive manometer, like the ones discussed in Sect. 13.1, filled with a mixture of liquid and solid ^{3}He. With a typical pressure resolution of $10\,\mu\mathrm{bar}$, the precision of temperature measurement is 3×10^{-4} at 1 mK, 3×10^{-5} at 10 mK and 5×10^{-6} at 100 mK (Fig. 11.1), [12.25]. The standard uncertainties of the temperature scale PLTS-2000, which is based on ^{3}He melting pressure thermometry are, of course, substantially worse; they are given in Sect. 11.3.

The ^{4}He impurities shift the minimum of the ^{3}He melting curve and change its slope. However, these effects are negligible at low ^{4}He impurity concentrations due to preferential adsorption of the heavier isotope on walls and due to phase separation at low temperatures (7.2). At higher ^{4}He concentrations, the effects can become noticeable. They are $\Delta P_{\min}/P_{\min} \approx 0.1$ bar for $x_4 = 2\%$, and the temperature errors in melting curve thermometry would be in the several percent range for such concentrations [12.26]. In addition, high magnetic fields depress the ^{3}He melting curve [12.27–12.29] because the entropy

of the solid phase is field dependent due to partial alignment of the nuclear moments of ^{3}He by the field. The equation for the field depression is

$$\Delta P = -a_2(T)B^2 - a_4(T)B^4, \tag{12.4}$$

with the temperature dependent functions a_i given in [12.29]. Typical values are $\Delta P \approx 0.25(0.15)$ bar at 3.5 (10) mK in a field of 10 T. A typical resulting temperature error in ^{3}He melting curve thermometry would be $\Delta T/T \approx 2\%$ at 25 mK and 5 T [12.29], which is much smaller than typical impacts of magnetic fields on resistance thermometers, for example (see Sect. 12.5).

The advantages of a ^{3}He melting pressure thermometer are the high resolution (about 1 μK) and reproducibility (several ppm), essentially zero power dissipation, insensitivity to RF radiation and (almost) to magnetic fields. A drawback is the rather large specific heat of liquid ^{3}He in the thermometer, the need of ^{3}He, of a fill capillary, and of a gas-handling system. A further advantage of the ^{3}He melting curve as a temperature scale is the fact that it can easily be transferred between laboratories without requiring the exchange of calibrated devices. It has therefore become for the millikelvin temperature range what the helium vapour pressure curves had already become for the Kelvin temperature range (Sects. 11.2, 12.2). Very careful new determinations of the ^{3}He melting pressures were discussed in Sect. 11.3. In particular, the detailed discussion of possible error sources for the pressure calibration (hydrostatic head, thermal expansion, etc.) in [12.20, 12.22] is illuminating for everyone interested in careful pressure measurements.

A high-resolution ^{4}He melting-pressure gauge for use near 2 K has been described in [12.30]; it is stable to a few 10^{-9} K over several hours.

12.4 Thermoelectricity

If the ends of a metallic wire are at different temperatures a voltage will develop along the wire. This voltage ΔU is the absolute thermoelectric force; the corresponding thermoelectric power is defined as

$$S = \frac{\Delta U}{\Delta T}\,. \tag{12.5}$$

Generally the thermoelectric power between two different metals is measured with a reference junction at a reference temperature, usually at 0°C to avoid influences from the contacts at the voltmeter (Fig. 12.3).

The advantages of thermometry based on thermoelectric power are: it is a local measurement using a point sensor; the device and the measurement are simple (but see below); the device is rather insensitive to magnetic fields (except for magnetic alloys, see below); the device has a small specific heat; the measurement occurs essentially without heat input; the results are reproducible, because in general there is no change even after the device has been warmed up and cooled down repeatedly.

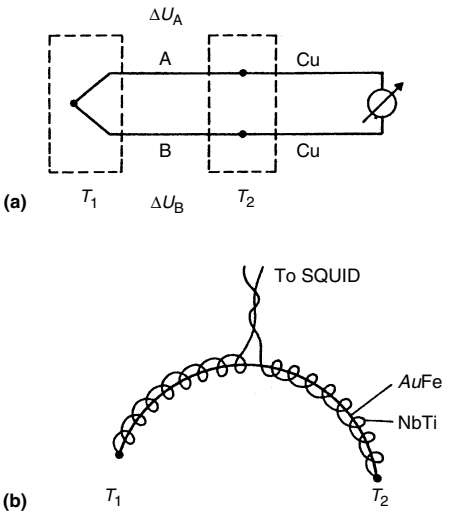

Fig. 12.3. Wiring for thermoelectric thermometry. (**a**) The general setup, where the thermoelectric power is created at the welded junction between wires A and B, which is at a temperature T_1. These two wires are connected to the Cu leads which eventually lead to the measuring instrument. (**b**) Wiring suitable for thermoelectric thermometry at very low temperatures. Here the thermopower of a wire of AuFe, for example, is compared to that of a superconducting wire of NbTi, which does not create any thermopower. At low temperatures the small thermopowers have to be measured with a SQUID

Unfortunately the thermoelectric power vanishes for $T \rightarrow 0$. Therefore, thermometry based on thermoelectric measurements with one of the usual combinations of thermocouple wires – for example, Constantan/Cu – becomes insensitive below 10 K (Fig. 12.4). However, new materials and very sensitive voltage measuring devices have been developed allowing thermoelectric thermometry to be extended even to the millikelvin temperature range. The newly developed suitable alloys are highly diluted magnetic systems like Au + a few up to several 100 ppm Fe [12.1, 12.2, 12.31–12.34], or Pd + a few up to several 100 ppm Fe [12.35–12.38]; usually commercially "pure" Au or Pd contain enough Fe. The first is a so-called Kondo alloy, where the magnetic moment of Fe in the Au matrix is strongly temperature dependent. Values for its thermoelectric power can be found in [12.1, 12.2, 12.34], see Fig. 12.4. It has been investigated in detail in [12.34] at 10 mK (here, $S = 10\,\mathrm{nV\,K^{-1}}$) to 7 K showing that the optimum Fe concentration is 300 ppm (Fig. 12.5). Of course, these still small voltages cannot be measured relative to a reference point at 0°C, because there the thermopower is very large so that the reference temperature would have to be extremely well regulated. For these low-temperature thermocouples the reference junction is usually kept in a liquid ^{4}He bath at 4.2 K. The

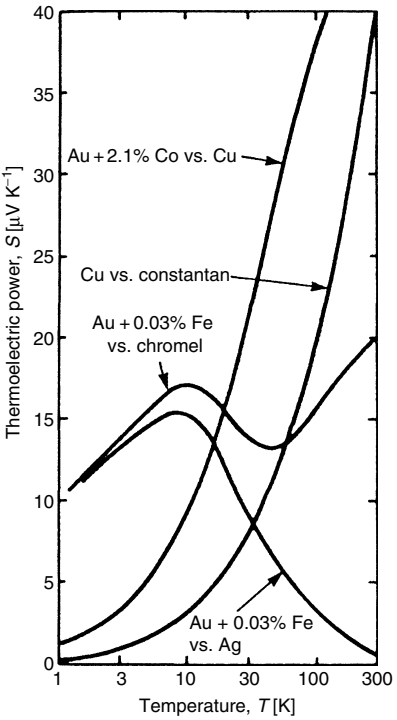

Fig. 12.4. Thermoelectric powers of some metal pairs [12.1]

second alloy, whose thermopower is shown in Fig. 12.6, is a so-called giant moment spin glass. Here the Fe impurity polarizes the highly paramagnetic Pd matrix, giving rise to a giant magnetic moment of up to $14\mu_B$. These giant moments freeze in at low temperatures with statistical orientations ("spin glass freezing") [12.37, 12.38]. Of course, the properties of these dilute magnetic systems depend strongly even on small magnetic fields [12.37, 12.38].

Spurious thermoelectric voltages may develop in a wire due to chemical inhomogeneity or physical strain if it is exposed to a temperature gradient; these effects in the leads to room temperature may be larger than the desired low-temperature signal from the junction. The leads have therefore to be carefully selected and fixed when they have to be brought out to room temperature. To avoid nuisance thermopowers one should join the various metals without using a third metal. Welding is the most appropriate joining procedure for a thermocouple. Very often thermopowers are a problem if one has to measure small voltages, because thermopower develops at soldering joints, at switches, and other contacts between different metals. Therefore sensitive measurements, for example in bridges, mostly have

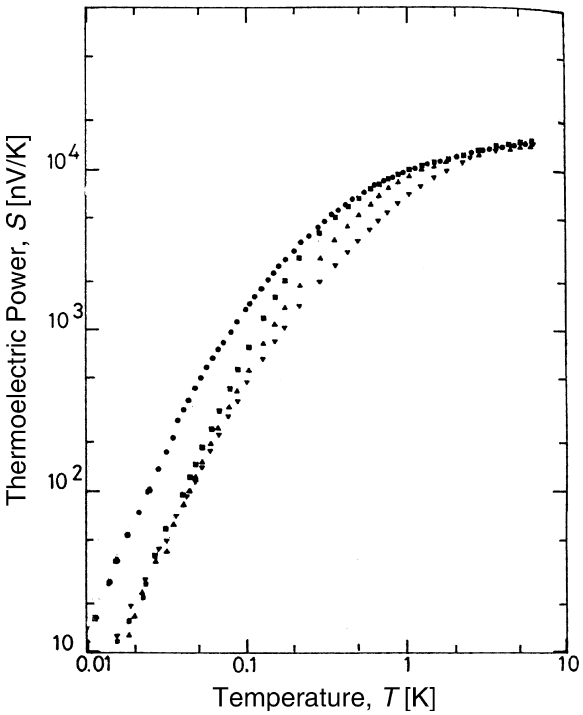

Fig. 12.5. Thermoelectric power of $AuFe_x$ alloys with Fe concentrations $x = 56$ ppm (▲), 123 ppm (■), 300 ppm (●), and 700 ppm (▼) as a function of temperature [12.34]

to be AC measurements. Because no voltage drop can be developed along a superconducting wire, a superconductor, for example NbTi, with $S = 0$ is the appropriate reference wire in a low-temperature thermocouple (Fig. 12.3b). The high-sensitivity device for measuring very low thermoelectric voltages at low temperatures is the so-called Superconducting Quantum Interference Device (SQUID), allowing a resolution of 1 μK at 1 K with a Au + 0.03 at.% Fe thermocouple, which has a thermopower of about $-9\,\mu V\,K^{-1}$ at 1 K [12.1, 12.2, 12.10, 12.31–12.33].

Generally, a practical low-temperature limit for the use of thermocouples is 10 K, with some effort and the use of magnetic alloys the temperature range can be extended to about 1 K, and the practical limit for thermoelectric thermometry is about 0.1 K. It has been shown that, in principle, thermopower can be used for thermometry to about 10 mK (Fig. 12.6). This has not been applied in routine temperature measurements because there are more suitable methods available, which will be discussed in the following sections. However, thermoelectric thermometry can be attractive in situations where temperature differences have to be measured.

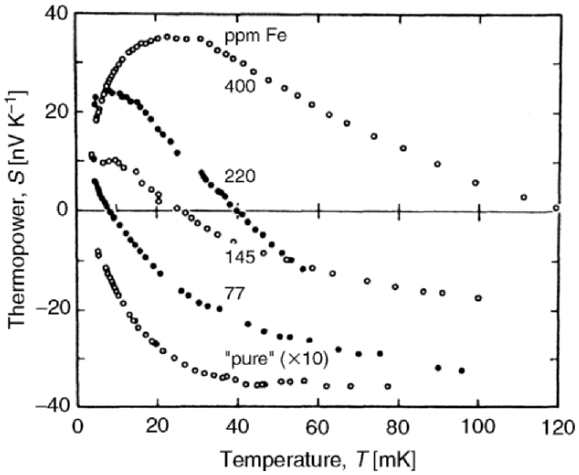

Fig. 12.6. Thermoelectric power of Pd doped with the indicated amounts of Fe (in ppm) as a function of temperature at millikelvin temperatures. The values for the "pure" sample have been multiplied by 10 for clarity [12.36]

12.5 Resistance Thermometry

Resistance thermometry is based on the temperature dependence of the electrical resistance of metals, semiconductors or complicated compounds (see below). It is probably the simplest and most widely used method of low-temperature thermometry. The devices are readily available and the measurements are easy. As we will see below, the problems at very low temperatures are thermal conductivity, thermal contact, and self-heating of the device due to the measuring current and RF absorption. In addition, the resistivity usually has no simple, a priori known temperature dependence, therefore a resistance thermometer is a secondary thermometer. Many different kinds of resistance thermometers are commercially available, often even calibrated for a particular temperature range.

12.5.1 Metals

The pure metal most commonly used for resistance thermometry is platinum [12.1, 12.9–12.11]. It is one of the standards for interpolation between fixed points of the ITS-90 (Sect. 11.2). Platinum is chemically resistant; it can be obtained with high purity (diminishing the temperature-independent residual resistivity part); it is ductile, so it can be drawn into fine wires; and its resistance has a rather large temperature coefficient. The temperature-dependent resistance of a commercial Pt-100 thermometer shown in Fig. 12.7 illustrates the linear R–T dependence over an appreciable temperature range. A Pt-100 thermometer is a platinum resistor with a resistance of exactly

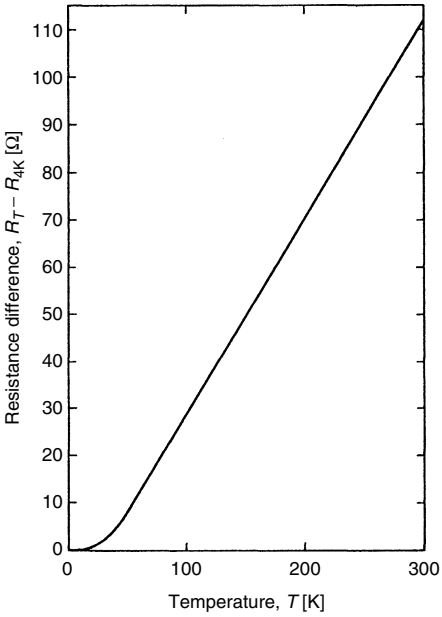

Fig. 12.7. Difference of the resistances at temperature T and 4 K of platinum as a function of temperature. The resistance difference varies linearly with temperature between room temperature and about 50 K

Table 12.2. Temperature–resistance values of a Pt-100 resistance thermometer

T (K)	10	15	20	25	30	40	50	60	77(!)	100
R(Ω)	0.09	0.19	0.44	0.94	1.73	4.18	7.54	11.45	18.65	28.63
T (K)	125	150	175	200	225	250	273.2(!)	300		
R(Ω)	39.33	49.85	60.23	70.50	80.66	90.72	100.00	110.63		

(For more data points see [12.1])

100 Ω at 0°C. Values at other temperatures are given in Table 12.2. Pt-100 thermometers or Pt thermometers with other resistance values are available commercially with calibration tables. They are well annealed and either fused in quartz glass or encapsulated in a quartz or metal tube which is filled with helium gas for thermal coupling of the Pt wire to its surroundings. It is rather important that the Pt wire is supported strain-free so it does not change its properties on repeated cooling and warming. Cheaper Pt thermometers are manufactured by lithographic techniques as metal films.

As can be seen from Figs. 12.7 and 12.8, sensitive thermometry with a Pt resistor or with other pure metals is only possible down to about 10 K; at lower temperatures we are in the temperature-independent residual resistivity range. As in the case of the thermopower, one can increase the sensitivity

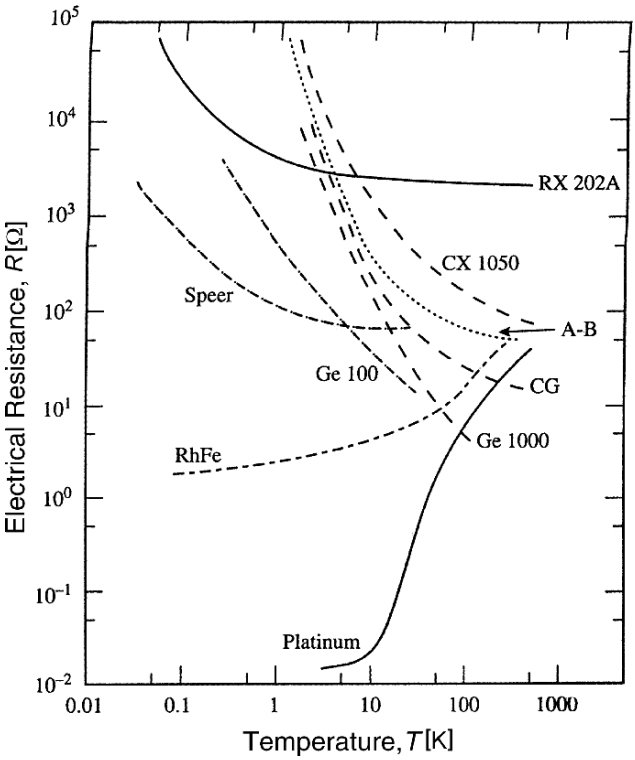

Fig. 12.8. Temperature dependence of the electrical resistances of some typical low-temperature thermometers. A–B denotes an Allen–Bradley carbon resistor, Speer is also a carbon resistor and CG is a carbon-in-glass thermometer; Ge 100 and Ge 1000 are two commercial germanium thermometers; CX 1050 is a CERNOX and RX 202A is a RuO_2 commercial thermometer (see below). The lower two curves are for the two indicated metals. Reprinted from [12.1], copyright (2002), Oxford Univ. Press

of the resistance of a metal to temperature changes at low temperatures by introducing magnetic impurities. This is shown for Cu with Fe impurities in Fig. 3.25. Like *Au*–Fe, the alloy *Cu*–Fe is a Kondo alloy, where the Fe moment is strongly temperature dependent at low temperatures, leading to an *increase* of the resistance with decreasing temperatures below about 15 K. The magnetic alloy most widely used for resistance thermometry at low temperatures is the commercially available alloy *Rh*–0.5% Fe [12.8,12.10,12.11]. Above 30 K its resistance behaves similarly to Pt, whereas below 10 K its resistance remains sensitive to temperature changes due to magnetic scattering of conduction electrons at the Fe impurity atoms; it then decreases almost linearly with decreasing temperature at $0.1\,\mathrm{K} < T < 1\,\mathrm{K}$ (Fig. 12.8). *Rh*–Fe resistance thermometers are also in use to realize temperature scales (Sect. 11.3.1)

and to transfer them between various laboratories. They show a stability of 10 mK/year and can be obtained commercially as incapsulated wires or thin film thermometers.

12.5.2 Doped-Germanium and Carbon Resistors

The resistance of a semiconductor does not *decrease* with temperature as it does for a pure metal; it *increases* with decreasing temperature because of the decreasing number of carriers. For an "ideal" intrinsic semiconductor the temperature dependence is given by

$$R(T) = \alpha \ \exp\left(\frac{\Delta E}{2k_{\mathrm{B}}T}\right) , \tag{12.6}$$

where ΔE is the energy gap between the valence and conductance bands, and α contains the weakly temperature-dependent mobility of the carriers. However, the resistance of semiconducting materials used for thermometry usually does not agree with this relation, and empirical equations between R and T have to be used. One can reach very high resistances and, above all, very high sensitivities at low temperatures where the conductivity is no longer intrinsic ($\Delta E \gg k_{\mathrm{B}}T$) but results from impurities donating or accepting electrons. Actually, very often the resistance of a semiconductor becomes too high below 1 K to be suitable for a temperature measurement. Resistance thermometry with semiconductors is an important and widely used secondary thermometry technique in the temperature range between about 10 mK and 10 K. Two favorite materials are germanium, specifically doped for low-temperature thermometry, and carbon in the form of commercial carbon resistors from the electronics industry.

Doped Germanium

Germanium used as a low-temperature thermometer is specially doped with 10^{15}–10^{19} atoms cm^{-3} of As ("n-type") or Ga ("p-type"). Below 100 K the conductance is due to holes or electrons which the dopant delivers. Such a thermometer is particularly suited for the temperature range $0.3\,\mathrm{K} \leq T \leq 40\,\mathrm{K}$. At lower temperatures the resistance often becomes too large ($> 1\,\mathrm{M\Omega}$), but with special doping these thermometers have been used to 30 mK. The temperature dependences of various Ge thermometers are shown in Figs. 12.8 and 12.9.

A great advantage of the germanium thermometers is the stability of their resistance values. Even after repeated cyclings between room temperature and low temperatures, or after an extended time on the shelf, the deviations at 4 K are typically only about 1 mK or, more generally, about 0.1%. Therefore these thermometers can be bought calibrated with a computer fit for the resistance–temperature relation to 50 mK (but this increases their price by at least an order of magnitude!). Such a computer fit has to be performed, because, unlike

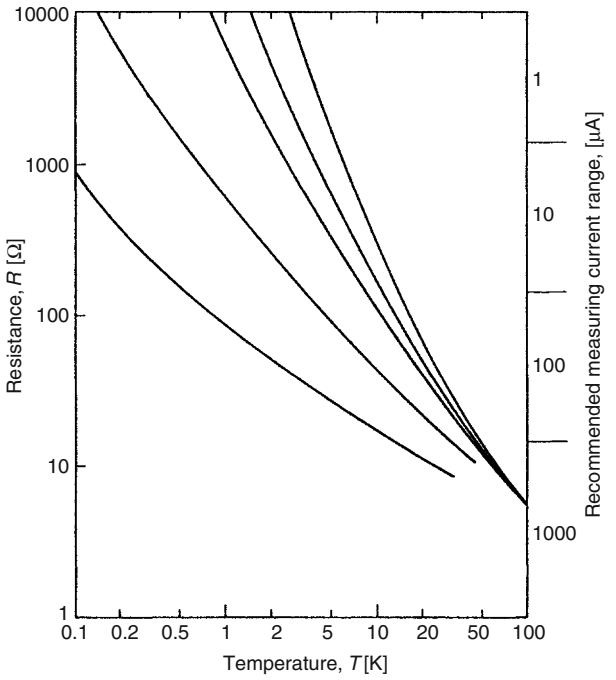

Fig. 12.9. Typical temperature dependence of the resistances of some commercial germanium thermometers. The right-hand vertical scale shows the measuring current recommended for these thermometers to avoid overheating them

an "ideal" semiconductor, the T–R relation for a heavily doped germanium thermometer is not simple, but given, for example, by

$$\ln R = \sum_{n=0}^{m} \alpha_n (\ln T)^n \text{ or } \ln T = \sum_{n=0}^{m} \beta_n (\ln R)^n \,. \tag{12.7}$$

To assure the reproducibility and stability of the device, the encapsulated single crystal Ge chip has to be supported strain-free on its four gold leads (Fig. 12.10). Again, for an encapsulated Ge thermometer the thermal coupling is provided by helium exchange gas as well as by its leads. This coupling and the thermal conductivity of the chip are weak. Therefore one has to keep the measuring current and hence the Joule heating low. Typical, safe values for the allowed measuring current and power are 10 (1; <0.1) μA and 10^{-7} (10^{-10}; $<10^{-12}$) W at 10 (2; <1) K. Another point of importance is the strong and orientation-dependent magnetoresistance of germanium thermometers, which increases with temperature sensitivity (Fig. 12.11) [12.39, 12.40]; at low temperatures they should not be used in the Tesla field range.

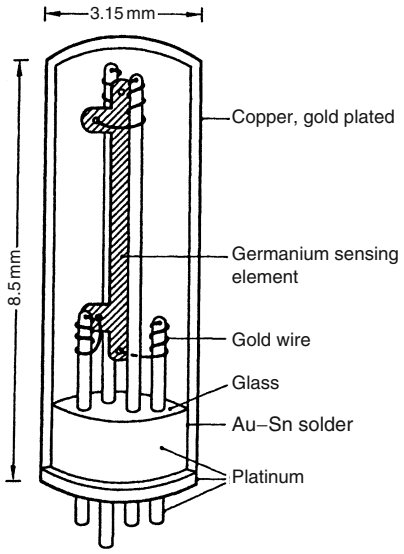

Fig. 12.10. Typical construction of a commercial germanium thermometer

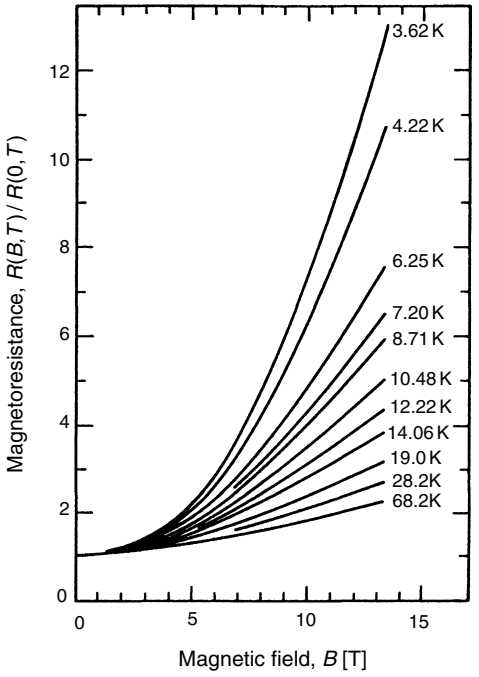

Fig. 12.11. Magnetic field dependence of the electrical resistance of a germanium thermometer ($R_{4K} = 856\,\Omega$) at the indicated temperatures [12.39]

Carbon Resistance Thermometers

In contrast to Ge thermometers, carbon composition resistors applied for low-temperature thermometry are not specially manufactured for thermometry but are taken from the mass production of the electronics industry. Therefore their price is less than 1 € each, which is two orders of magnitude lower than the price of the specially produced Ge thermometers. Due to this low cost and their very suitable R–T behavior, carbon resistance thermometers were for a long time the most widely used secondary thermometers in the upper millikelvin and Kelvin temperature ranges.

Pure carbon is not a semiconductor. The negative R–T characteristic of commercial carbon resistors results from their production process, which consists of pressing and sintering fine carbon particles together with some glue. The resistance is probably mostly determined by the contact resistance between the particles and by composition. Particle size and production method have an essential influence on the behavior of carbon resistors. As a result, the resistance of carbon resistors changes from sample to sample and often is not very reproducible after thermal cycling due to the stresses involved. Furthermore, they show ageing and sometimes even changes during a low-temperature experiment. The typical drift in resistance of a carbon thermometer is of the order of 10^{-3} per time decade [12.41, 12.42]; no time dependence has been observed for germanium-resistance thermometers. One therefore should repeatedly cycle a carbon resistor between room temperature and liquid-nitrogen temperature before using it as a thermometer. And one has to avoid overheating it while soldering on its short leads. Anyway, the calibration should be repeated in each run if temperature has to be measured to within a few percent or even better.

For low-temperature thermometry almost exclusively the following three commercial types of carbon thermometers with the given properties were in use:

Allen–Bradley 1/8 W; small, cheap; good at $T > 1$ K; too large R (and $\mathrm{d}R/\mathrm{d}T$) at lower T [12.4, 12.43].

Matsushita 1/8 W; types ERC 18 GK and ERC 18 SG; small; useful at $T \geq 10$ mK [12.44–12.46].
Speer 1/2 W; type 1002; larger; particularly useful in the millikelvin temperature range to about 10 mK because they have a less steep R–T dependence [12.47–12.49].

Typical temperature dependences of the resistance of these thermometers are shown in Figs. 12.12–12.15. With such thermometers, a resolution of order 10 μK at $T \leq 1$ K is possible. The particular type most suited for the desired purposes – most importantly the temperature range of interest – has to be chosen.

Application of carbon thermometers for thermometry *below* 1 K presents some problems. These are their rather high heat capacity (Fig. 12.16) and

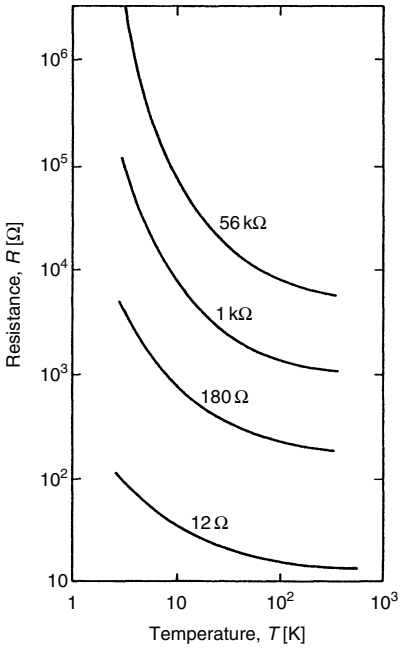

Fig. 12.12. Temperature dependence of the resistances of four Allen–Bradley carbon resistors (1/8 W) with the indicated room-temperature resistances [12.43]

their low thermal conductivity. These two intrinsic properties, as well as the difficulty of thermal coupling of the thermometers to their environment while avoiding electrical contact can lead to very long thermal relaxation times [12.49] and, even worse, to thermal decoupling from their environment. This may lead to saturation of the resistance at low temperatures, mostly due to pick-up of RF noise (Fig. 12.15). Typical values for the thermal resistance of Speer resistors are $R \simeq 10^4 T^{-3} (\mathrm{K\,W^1})$ [12.48]; in this reference it was shown that the bottleneck for Speer carbon resistors is the thermal resistance in the carbon itself rather than the Kapitza boundary resistance.

The most difficult problem for carbon thermometry in the millikelvin temperature range is therefore establishing thermal equilibrium within the thermometer and between the thermometer and its surroundings. The problem of coupling these thermometers thermally to the area whose temperature is supposed to be measured has the consequence that joule heating from the measuring current or due to pick-up of RF waves has to be kept very small. As a general rule the heat input to the thermometers should be at most

$$\dot{Q}(\mathrm{W}) < 10^{-6}\, T^4\ (\mathrm{K}^4)\,, \tag{12.8}$$

if overheating of the resistor is to result in a temperature error of not more than about 1%. This limit gives, for example, $\dot{Q} < 10^{-14}\,\mathrm{W}\,(10^{-10}\mathrm{W})$ for

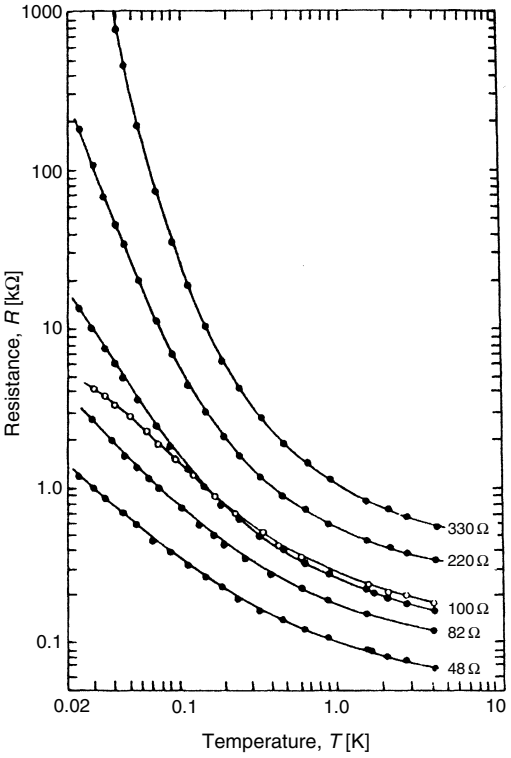

Fig. 12.13. Temperature dependence of the resistances of several Matsushita carbon resistors (grade ERC-18 SG, 1/8 W) with the indicated room temperature resistances (•). For comparison the temperature dependence of a Speer carbon resistor (grade 1002, 1/2 W, 100 Ω) is shown as open points [12.45]

a well-shielded and well-coupled piece of carbon at 10 mK (100 mK) [12.43, 12.48, 12.50, 12.51].

For the Kelvin temperature range it is adequate to put the carbon thermometer into a tightly fitting hole filled with vacuum grease (Fig. 12.17a) [12.57] or to glue it into a Cu foil for thermal contact (Fig. 12.17b). However, these thermometers should not be used in their original form if temperatures below 1 K are to be measured. For the millikelvin temperature range one should use carbon slices about 0.1 mm thick to achieve adequate thermal response and contact [12.50, 12.51, 12.58]. For this purpose first the phenolic cover should be removed from the resistor. Then one side of the carbon core should be ground down with fine sandpaper. The resulting semicircular piece of carbon can be glued to a Cu sheet (separated by a thin cigarette or lens paper) for mechanical strength and for better thermal contact. Then the second side of the carbon can be ground down to a remaining thickness of 0.05–0.1 mm (or a resistance of 1–2 kΩ if Speer resistors are used), see Fig. 12.17c. Finally a

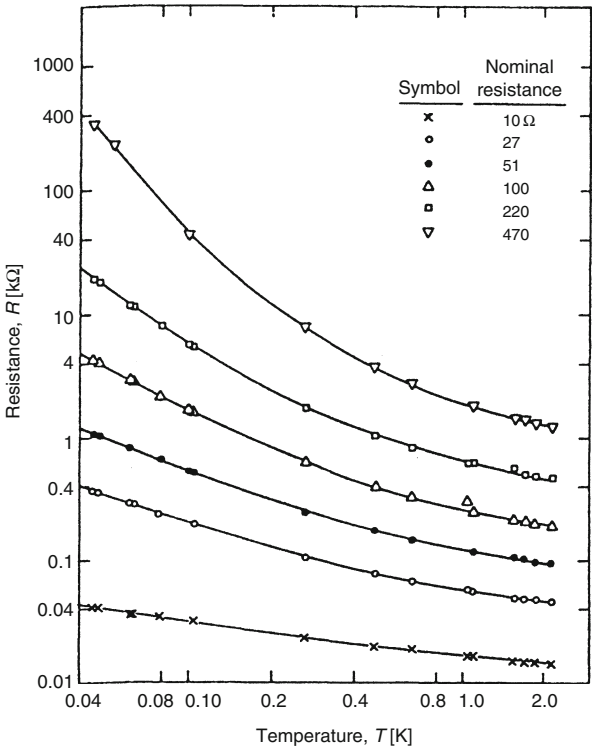

Fig. 12.14. Temperature dependence of the resistances of various Speer carbon resistors (grade 1002, 1/2 W) with the indicated room temperature resistances [12.47]. For more recent data for the 220 R and 470 R units at 50 mK to 300 K see [12.49]

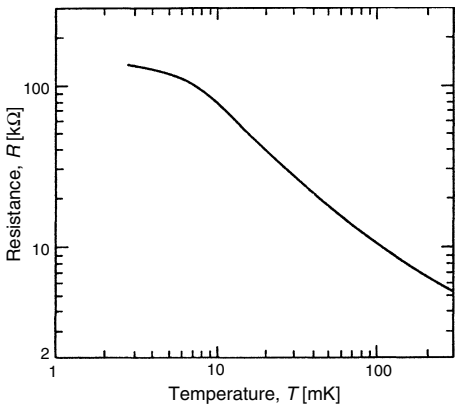

Fig. 12.15. Temperature dependence of a ground-down Speer carbon resistor (Fig. 12.17c). The resistance seems to saturate below about 7 mK due to a heat input of about 10^{-14} W from the measuring current and from the RF-noise pick-up [12.50]

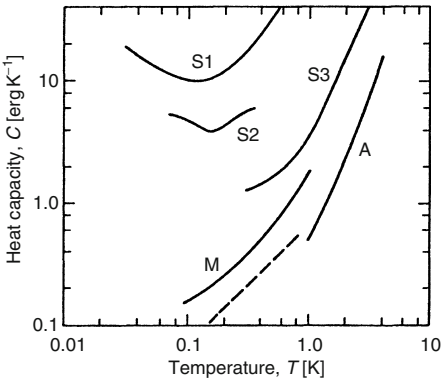

Fig. 12.16. Heat capacity of modified carbon resistors. S1 Speer 220 Ω (about 30 mg) [12.52]; S2: Speer 220 Ω (25 mg) [12.53]; S3 Speer 220 Ω (17 mg) [12.54]; A Allen–Bradley 116 Ω (11 mg C and 2 mg Cu) [12.55]; M: Matsushita, 100 Ω (about 5.5 mg C and Cu each) [12.56]. The dashed curve is an estimate of the contribution of the copper leads to the heat capacity of the Matsushita resistor

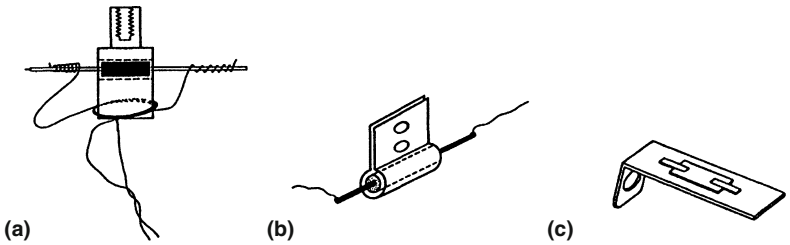

Fig. 12.17. Recommended designs for the use of a carbon resistor as low-temperature thermometers. For the Kelvin temperature range it is sufficient to put it in a hole of a Cu holder which can be filled with grease for thermal coupling [12.52] (**a**) or to glue the unmodified carbon thermometer into a Cu foil (**b**). The leads to the thermometer should be thermally heat sunk to the Cu holder. For the millikelvin temperature range one should use only a 0.1 mm thick slice of a carbon resistor to achieve adequate thermal contact (**c**). For this purpose one side of the resistor should be ground down. The remaining semicircular piece should then be glued with a thin layer of epoxy to a metal heat sink for protection against breakage (put a cigarette paper in between for electrical isolation). Then the second side of the resistor can be ground down to give the required thickness of the thermometer. It should then be covered with a copper foil for shielding against RF pick-up. The leads, of course, should again be heat sunk to the place whose temperature the carbon slice is supposed to measure. From there on the leads should be superconducting to reduce heat transmitted along them

thin Cu foil should be glued to the upper side for electrical and thermal shielding of the thermometer. The varnish or epoxy will penetrate the carbon, giving it a better mechanical stability and preventing microcracks. Such thermometers have been found to have much more reproducible characteristics than in

their original shape; they keep their calibration for years and through many cooldowns to within about 1%. The leads to the thermometer have to be well heat sunk at various points along their way in the cryostat and eventually to the area whose temperature is supposed to be determined; this, of course, applies to other resistance thermometer as well. Only with such a design, the sensitivity and the thermal coupling can be maintained even in the low millikelvin range (Fig. 12.15), and a thermal time constant of some minutes is possible even at 10 mK [12.51]. Of course, the temperature dependence of the resistance of a carbon thermometer is not simple; one has to fit an equation like (12.7) to obtain their $R(T)$ dependence. Carbon thermometers show an often non-monotonic magnetoresistance of typically only a few percentage per tesla [12.8, 12.10, 12.40, 12.44, 12.46, 12.59], see Figs. 12.18–12.20.

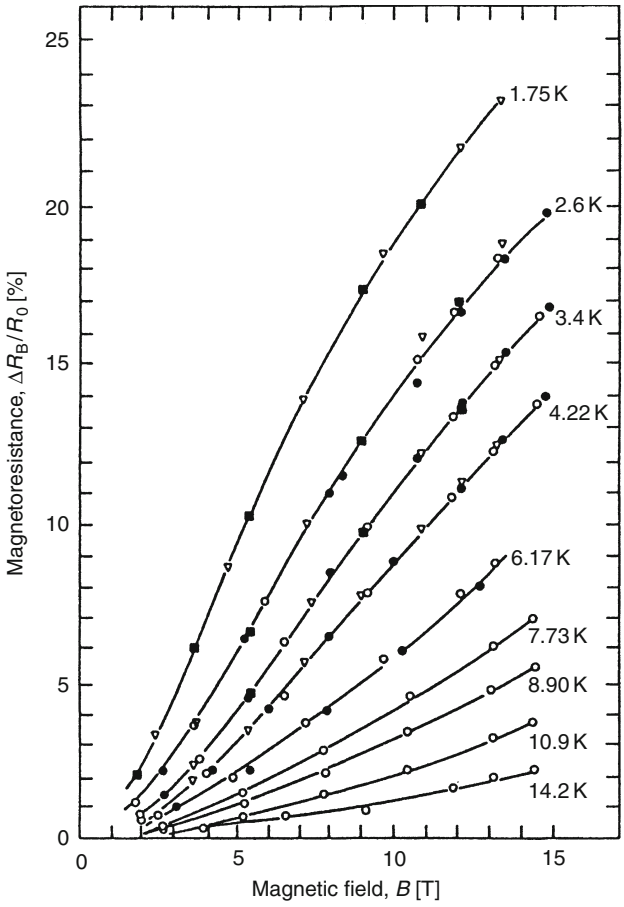

Fig. 12.18. Magnetoresistances of 47 Ω, 1/4 W Allen–Bradley carbon thermometers [12.40]

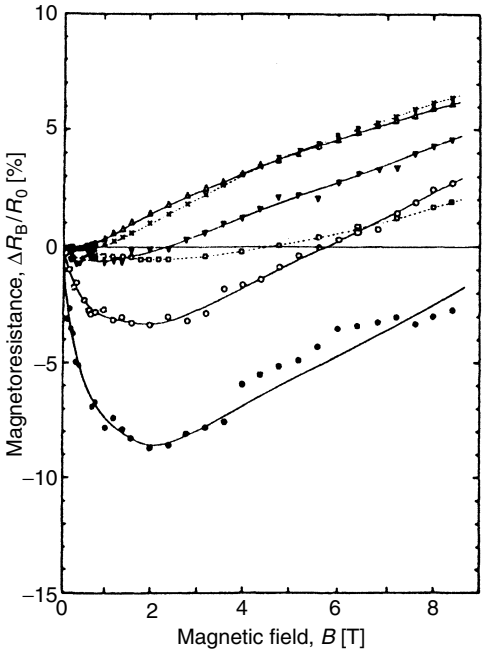

Fig. 12.19. Magnetoresistances of a Matsushita carbon resistor (68 Ω, 1/8 W) at 0.05 K (●), 0.1 K (○), 0.25 K (▽), 0.5 K (△), 1.0 K (x), and 4.2 K (□) [12.46]

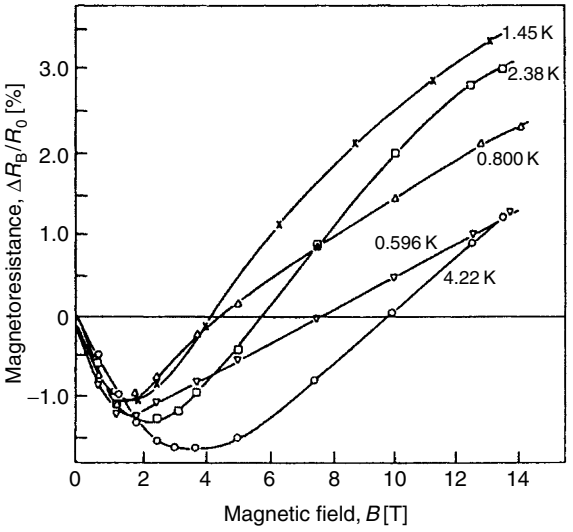

Fig. 12.20. Magnetoresistances of a 220 Ω, 1/2 W, grade 1002 Speer carbon resistor [12.40]. For more recent data for the 470 R unit see [12.49]

For the Speer resistors, the change of the resistance in magnetic fields of less than 10 T was reported to be less than 10% at 0.2–4 K [12.59] and for fields up to 18 T, to be less tan 12% at 0.1–1.6 K [12.49]. In general, they are not recommended for use in high magnetic fields; here the new oxide compound resistance thermometers to be discussed in Sect. 12.5.3 are surely preferable.

For decades, from the beginning of the 1960s to the end of the 1990s, these carbon resistors were the most widely used secondary low-temperature thermometers. Unfortunately, the mentioned three types of carbon resistors are no longer manufactured. For some time, they were available from stocks kept by some suppliers of cryogenic equipment. Interested users may still try there or with some colleagues who may still keep some of these very useful resistors in stock [12.9, 12.49, 12.60].

Because the carbon-composition resistors are no longer available, it is very fortunate that new (and even better suited) commercial, cheap resistance thermometers have become available. They are the thick-film chip RuO_2-based resistors for 30 mK $< T <$ 20 K and the ceramic zirconium oxynitride resistors for 0.1 (better only 1 K) to 400 K. I will discuss their properties in the next section.

12.5.3 Oxide Compounds: RuO_2 and Cernox Thermometers

Thick-Film Chip Resistors Based on RuO_2

The thick-film chip resistors based on RuO_2 [12.61–12.74] can be obtained from the relevant manufacturers of electronic components (Dale Electronics, Norfolk, Nebraska, USA; NV Philips, Eindhoven, Netherlands; ALPS Electric Comp., Japan; Siegert GmbH, Germany, for example; however, be careful: the composition and hence the properties of the resistors from some manufacturers seem to have changed with time) or from various suppliers of cryogenic equipment (see, for example [12.75]), or they can be homemade [12.76–12.78]. These resistors are metal-ceramic composites consisting of a mixture of conductive RuO_2 and Bi_2RuO_2 embedded in a lead silicate glass (PbO–B_2O_3–SiO_2) matrix, deposited on an alumina substrate and heated to above its glass point. The resulting negative non-metallic resistance characteristic (Fig. 12.21) depends mostly on the metal-to-glass ratio. Their advantages are reproducibility, weak magnetoresistance (see below), small size and mass (a few milligrams, making them useful for application in calorimeters), and low cost. For making thermal contact, they can be carefully epoxied or glued to a sample without indication of detrimental effects. Of course, if used in the millikelvin range, the low-temperature parts of the leads should again preferably be superconducting, well heat-sunk, and a low-pass filter (Fig. 12.28) should be installed on them. Resistors with room temperature values in the range of 0.5 to a few kΩ seem to be quite suitable for low-temperature thermometry with a sensitivity comparable to that of Ge resistance thermometers. Their resistance can be well fitted by the empirical equation [12.70]

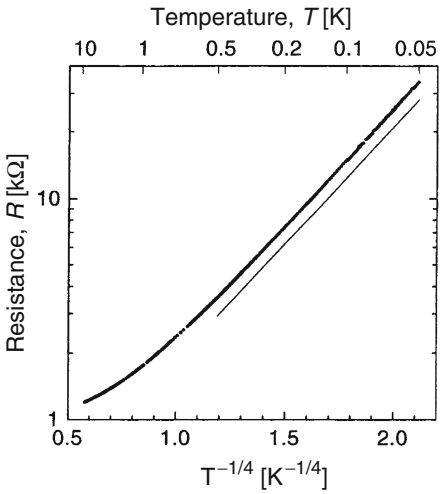

Fig. 12.21. Resistance of a commercial RuO_2-based resistor versus $T^{-1/4}$. This temperature dependence fits the data well between 0.05 and 0.5 K as indicated by the straight line. Reprinted from [12.72], copyright (2001), with permission from Elsevier. For commercial RuO_2 based resistors with different characteristics, see [12.75]

$$\ln R = \sum_{n=0}^{2} A_n \left(\ln T\right)^n . \tag{12.9}$$

In a limited temperature range, the expression

$$R = R_o \exp(T_o/T)^{1/4} \tag{12.10}$$

with the constants R_o and T_o depending on composition fits the data well [12.61–12.63, 12.66, 12.70, 12.71, 12.76–12.78], (Fig. 12.21). This dependence corresponds to an electronic conduction mechanism due to variable-range hopping in three dimensions between localized states near the Fermi energy with a constant electronic density of states. The temperature range can be extended by using somewhat larger exponents [12.61, 12.63, 12.65, 12.66, 12.70, 12.71,12.76–12.78], (Fig. 12.22), indicating a crossover to an exponent 1/2 due to possible influences from Coulomb interaction, which leads to a gap in the density of electronic states at the Fermi energy.

Several researchers have investigated the magnetoresistance of these thermometers [12.61–12.67, 12.70–12.74]. The results do not agree in detail and they seem to depend somewhat on the batch. However, for most of them, the magnetoresistance is negative for fields up to about 1 T, then goes through a broad minimum, and is positive at higher fields (Fig. 12.23). The magnetoresistance becomes larger and the size of the minimum becomes more pronounced with decreasing temperature. The resistance change from the zero field value to the resistance minimum at about 1 T (at 8 T) is typically less than 1(5)%

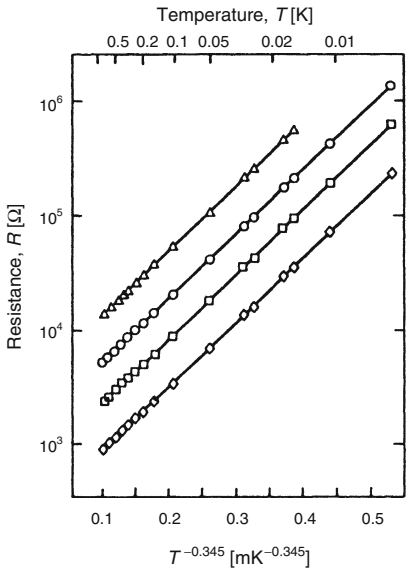

Fig. 12.22. Resistances vs. $T^{-0.345}$ of four different RuO_2 resistors with approximate room temperature values of 0.5 kΩ (◊), 1 kΩ (□), 2 kΩ (○), and 4.7 kΩ (△), respectively. The *upper* horizontal scale shows the temperature in Kelvin [12.65]

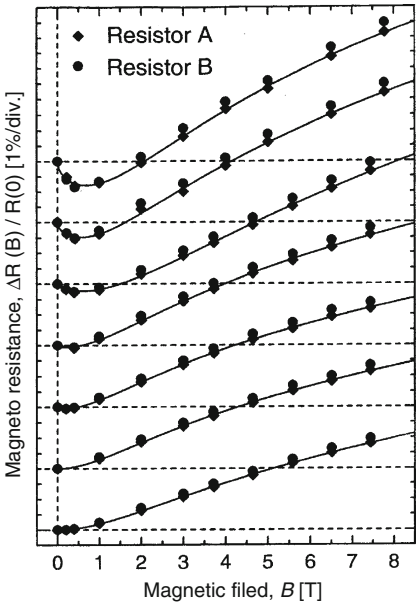

Fig. 12.23. Relative change of the resistance of a two commercial RuO_2-based resistors as a function of magnetic field at 0.05, 0.06, 0.09, 0.12, 0.16, 0.20, and 0.24 K (from top to bottom). The origin of each data set is offset for clarity. Reprinted from [12.72], copyright (2001), with permission from Elsevier

of the zero field value at 0.5 K; at 30 mK these changes are about 4(10)% of the zero field value [12.70–12.72]. However, larger values have also been reported [12.73,12.74]. The magnetoresistance at temperatures $T > 1$ K fortunately is less than 1% for $B < 8$ T [12.70,12.71], which is important for many applications. A dependence of the magnetoresistance proportional to $B^{1/2}$ has been discussed in [12.72,12.73]. In [12.63] and [12.73], the magnetoresistance has been investigated to 20 and 32 T, respectively.

Schottky-type anomalies (Sect. 3.1.5) in the heat capacity of commercial thick-film chip resistors have been observed in measurements at $0.01\,\mathrm{K} < T < 2\,\mathrm{K}$ with a peak at 0.4 K [12.69]. The observed maximum corresponds to $C_{max}/\mathrm{mass} = 30\,\mu\mathrm{J\,K^{-1}\,mg^{-1}}$ (Fig. 12.24). The origin may be magnetic impurities in the alumina substrate, which could be removed or thinned for calorimetry experiments, for example [12.64,12.69].

These resistors change their values during about the first 60 thermal cycles, but become very stable afterward according to [12.63, 12.73]. Hence, they should be calibrated only after such a number of thermal cycles have been performed. When used in the millikelvin temperature range, the applied power should be 10^{-13} W or less to avoid overheating and if 1% accuracy is the aim [12.68,12.70,12.72].

In [12.76–12.78], it is reported how such thermometers can be home-made from commercially available RuO_2 paste using standard screen-printing techniques followed by drying and firing. Both the R–T characteristics and the sensitivities can be adjusted by changing the printing geometry and composition. They have been investigated to 50 mK [12.76]. In [12.77,12.78], a detailed investigation of the dependence of the properties of these home-made resistors on their composition, in particular the crossover from the above-mentioned

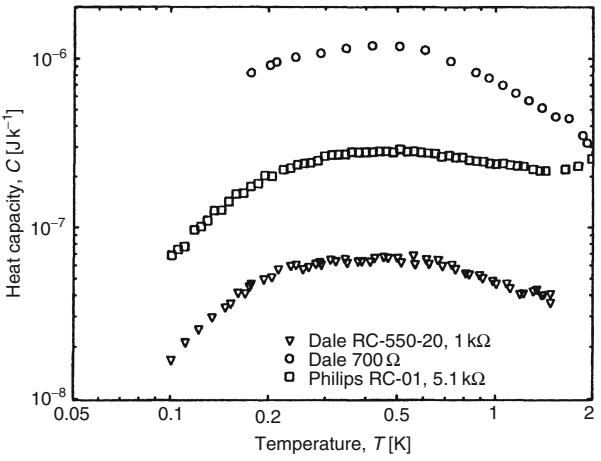

Fig. 12.24. Heat capacity of thick-film chip resistors based on RuO_2 [12.69]

exponent 1/4 to an exponent 1/2 by changing temperature and/or composition, has been presented. The properties are in general comparable to those of the commercial resistors.

Thin-Film Ceramic Zirconium Oxynitride (CERNOX) Resistors

The "CERNOX" thermometers [12.75, 12.79–12.81] are manufactured commercially by reactive sputter deposition of zirconium in an atmosphere containing Ar, N_2, and O_2 onto a sapphire substrate of about 0.3 mm thickness. The resulting zirconium oxynitride film has a thickness of about 0.3 μm. The negative temperature characteristic (Fig. 12.25) can be varied by adjusting the partial pressures of the gases. The electrical conductivity changes from metallic to semiconducting behavior with increasing O_2 content because oxygen will be incorporated into the ZrN lattice, which is enlarged by this incorporation. The thermometers are available with different packaging options and with temperature sensitivities $(T/R)(\mathrm{d}R/\mathrm{d}T)$ between about −0.6 and −3, although units having the range −1.2 to −1.9 with resistance values of 1–10 kΩ at 4.2 K are recommended for thermometry [12.79]. Their properties make them good, fast thermometers from 0.1 K to even above room temperature, with only a small change in sensitivity. These sensors are robust, small (mass less than 3 mg, making them ideal for high-field – see below – heat-capacity measurements), ease of thermal contact, sensitive, have a fast response time (a time constant of less than 1 ms at 1.7 K was reported for a bare CERNOX resistor in [12.81]; however, the supplier gives a conservative value of 1.5 ms at 4.2 K for the device), low sensitivity to magnetic fields, and can be bought with calibration [12.75].

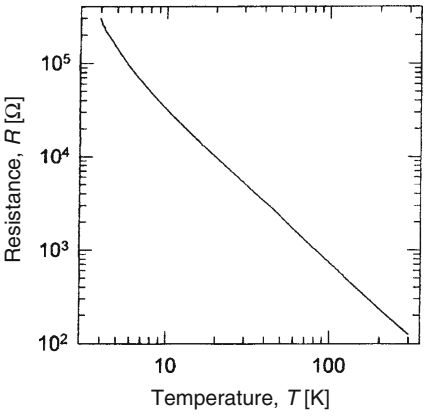

Fig. 12.25. Resistance of a commercial CERNOX resistor as a function of temperature: Reprinted from [12.81], copyright (1998), with permission form Elsevier. For commercial CERNOX resistors with different characteristics, see [12.75]

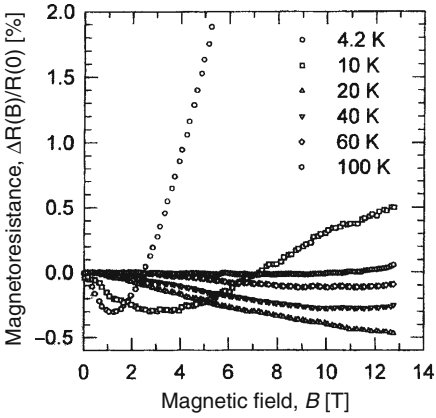

Fig. 12.26. Relative change of the resistance of a commercial CERNOX resistor (same whose data are shown in Fig. 12.25) as a function of magnetic field at the indicated temperatures. Reprinted from [12.81], copyright (1998), with permission from Elsevier

The weak dependence of the resistance of these sensors on magnetic field above 1 K has been investigated by a number of researchers [12.79, 12.81–12.83]. Similar to the above-discussed RuO_2 resistors, (as well as to the Matsushita and Speer carbon thermometers, see Figs. 12.19 and 12.20) there seem to be competing negative (dominating at low fields) and positive (dominating at higher fields) contributions to their magnetoresistance with a rather small net effect (Fig. 12.26). The change of resistance in fields up to 13 T is between 1 and 3% at 4.2 K and less than 0.5% at 10 K and above [12.79, 12.81, 12.82]. At 32 T, changes of less than 3% for temperatures above 4.2 K have been reported [12.79]. The magnetoresistance seems to depend on the individual sensitivities of the sensors. Above liquid nitrogen temperatures the magnetoresistance becomes so small that most users will not bother correcting for it, many may do so even at lower temperatures. *These resistors are probably the best choice for use in high magnetic fields at temperatures above 1 K.* However, below 1 K and at fields of 17 T, anomalously large resistance decreases have been observed in [12.83].

Procedures to correct for magnetic field dependences of resistance thermometers at low temperatures to better than 1% for fields up to 8 and 31 T, respectively, have been discussed in [12.84, 12.85].

Good overviews on the large variety of calibrated and uncalibrated commercial resistance thermometers including information on their sensitivity, stability, field dependence, and packing options as well as on the related electronics are given in [12.75].

12.5.4 Resistance Bridges

In low-temperature resistance thermometry one has to measure very small voltages, often in the nanovolt range, because low-temperature resistance

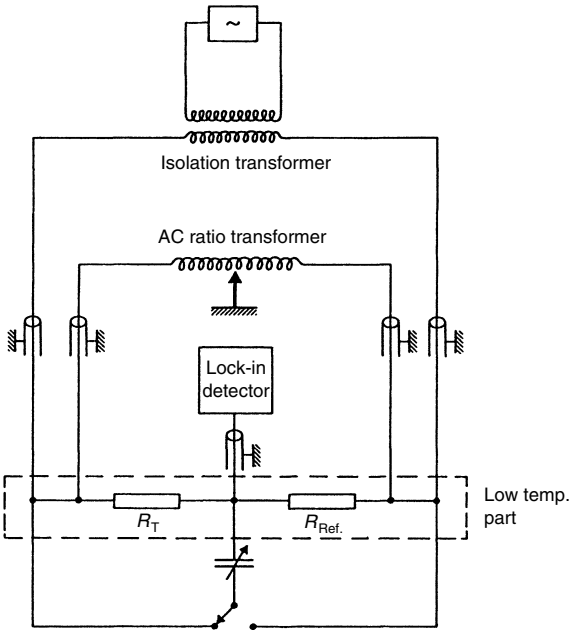

Fig. 12.27. Schematic diagram of a bridge for measuring the resistance of low-temperature thermometers. The adjustable capacitor is used to compensate a capacitive unbalance in the bridge [12.17]

thermometry has to be performed at very low powers (see earlier). Therefore, in general a direct current–voltage measurement is not applicable. The solution is to resort to a suitable bridge design for the electronic equipment [12.6, 12.17, 12.43]. In general, the so-called five-wire method is applied (Fig. 12.27) in order to separate current and voltage leads. In this way, the resistance of the leads is not measured along with the resistance of the thermometer. The measurement should be performed with AC current to avoid problems arising from thermoelectricity and to obtain higher sensitivities. The measurements are performed at low frequency, e.g., 40 Hz, to keep capacitive effects leading to out-of-phase signals at a low level. The simple design of the usual Wheatstone bridge has to be improved for adequate low temperature resistance thermometry. Some of the possible problems and possibilities for improvements are the following. One has to be very careful about grounding; ground loops have to be avoided to keep nuisance currents in the thermometer small. All leads and the thermometer have to be shielded from RF, because the thermometer often has a rather high resistance and, together with its leads, it may be well matched to absorb sizable amounts of RF energy floating around in the laboratory. Figure 12.27 shows a bridge design which avoids some of the problems that may arise with a standard Wheatstone bridge. In particular, it reduces the influence of the resistances r_i of the leads on the cold sensor

because the equation for the resistance R_T of the thermometer is given by

$$R_T + r_1 = R_{Ref} + r_2 \,, \tag{12.11}$$

whereas for a simple Wheatstone bridge r_1 and r_2 both add to R_T. This design also decouples the AC-power supply from the bridge and it uses an inductive voltage divider ("ratio transformer") to null the voltage across the bridge. A ratio transformer has a very small error per reading, is nearly unaffected by age, temperature and voltage, and it has a low impedance. The null detector is a phase-sensitive lock-in amplifier with a high voltage sensitivity. Finally, the reference resistor, which may be a stable metal film resistor, is kept at low temperatures to keep its resistance constant and the lead resistances in the two arms of the bridge as equal as possible to reduce the noise signal and improve the stability. A variable capacitor is included to null out the out-of-phase signal. Such a bridge can be homemade, with the lock-in amplifier and the ratio transformer as the most expensive components, or one can buy an AC resistance bridge commercially. Some modern resistance bridges for thermometry do not use a reference resistor but compensate the voltage drop across the resistor using feedback electronics. In this way, it is possible to realize fully automatic bridges, that can be controlled and read out by a computer.

The leads into the cryostat should be twisted pairwise, rigidly fixed and well shielded to avoid induced currents due to movements in electromagnetic fields which are always present. In the low-temperature part they should be superconducting if the working range is $T < 1\,\mathrm{K}$ to keep the heat flow to the thermometer small, and they have to be thermally anchored, preferably at a temperature as close as possible or slightly below the temperature the thermometer is exposed to. This thermal anchoring of the leads can be performed by glueing them on a Cu rod to which a layer of lens or cigarette paper has been glued with GE 7031 varnish (diluted by a toluene–methanol mixture). The Cu rod should be well annealed to keep its thermal conductivity high.

Equipment for very low temperature experiments is very often installed in a shielded room. The main advantage of such a setup is not so much that the shielded room keeps RF power away from the refrigerator, but that it keeps RF power away from the leads and from the thermometers to avoid heating of the temperature sensors. A final step to keep nuisance RF heating to the low-temperature sensor at a tolerable level is to instal a low-pass filter at low temperatures just in front of the low-temperature resistive elements. A design of such a filter is shown in Fig. 12.28 [12.6, 12.43, 12.48, 12.51]. It should be kept in a cold Cu housing for shielding.

A very successful design of a thermometer made from a Speer grade 1002–100 Ω-1/4 W resistor with appropriate thermal anchoring and shielding of it as well as of its leads has been described in [12.51]. The thermometer is ground down to 0.15 mm and fixed with Stycast 1266 epoxy; it showed a response time of 5 min at its lowest useful temperature of 5 mK, where it still did not show any saturation effects, which is attributed to the cold filter, the careful electromagnetic shielding of thermometer and leads, and the small measuring power of 4 fW.

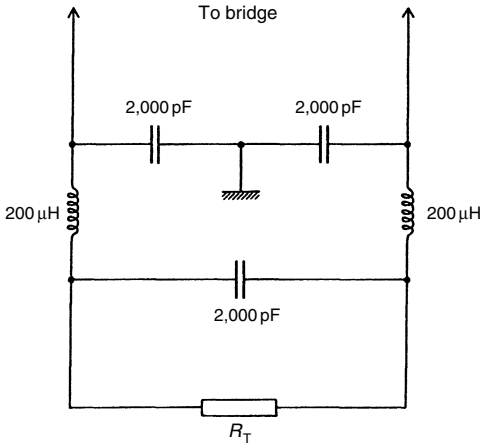

Fig. 12.28. Low pass filter between a resistor R_T used as a low-temperature thermometer and the bridge by which its resistance is measured. The cutoff frequency for the shown values of capacitors and inductances is about 0.1 MHz. The filter should be put into a Cu case to which all elements are well heat sunk. The inductances can be homemade and for the capacitors one could use commercial mica or, better, styroflex capacitors

12.6 Coulomb Blockade Thermometry

Modern micro- and nano-lithography, in particular electron-beam lithography, has opened the way to new concepts in thermometry with very small, very fast and even primary sensors. Because of their small size of order $1\,\mu m^2$, they measure the temperature locally – for example on the tip of a scanning tunneling microscope – they can be integrated into other micro-devices, and they can be fabricated reproducibly in large numbers in well-developed, controlled processes. However, one has to take into account that they allow only very small measuring powers to avoid self-heating and that the devices measure the *electron* temperature. The latter is particularly important at low temperatures because the heat transport between electrons and phonons decreases with T^5 ([12.86] and references in [12.87], p. 223), so that the electrons easily decouple thermally from the underlying lattice.

On one hand, important and well-developed micro-sensors are superconductor-insulator-normal metal (SIN) tunnel junctions. Their I-V characteristic depends on the temperature of the normal electrode only, yielding the Fermi distribution of the electrons as long as $T/T_c < 0.4$. They have a very steep tunneling characteristic at temperatures near to the superconducting transition temperature, which has made them attractive X-ray detectors, infrared bolometers, as well as thermometers for on-chip

micro-coolers (see Sect. 13.9). SIS junctions on the other hand have very high energy resolution and are therefore used as photon and particle detectors but not much as thermometric devices [12.87].

However, the most promising micro-thermometric sensor is the Coulomb blockade thermometer (CBT) using single-electron tunneling; their development has been mostly advanced by the work of Pekola and coworkers [12.87–12.91]. In this device, tunnel junctions are connected in series by metallic islands. If the resistance of the junctions is higher than the quantum resistance $R_Q = h/4e^2$, a well-defined number of electrons are located on the islands. At finite temperature, single electrons (or holes) can occasionally tunnel through the barrier of the junctions due to their thermal energy. Each extra electron increases the Coulomb charging energy E_C of the islands. For small junctions with small capacitances, E_C can exceed the ambient thermal energy and the Coulomb repulsion prevents the tunneling of additional electrons. This "Coulomb blockade" leads to a drastic decrease of the tunneling current at $k_B T < E_C$ and low bias voltages V so that e $V < E_C$.

A Coulomb blockade thermometer, however, is operated in the so-called weak Coulomb blockade regime ($k_B T \approx E_C$) where single-electron tunneling effects play a role and temperature influences the electric transport properties. In this regime, the I-V characteristic does not show a sharp Coulomb blockade gap but is smeared over the range e $V \sim k_B T$. One then has a competition between thermal energy $k_B T$, electrostatic energy e V at bias voltage V, and charging energy $E_C = e^2/2C^*$ due to extra or missing individual electrons on the metallic electrodes, where C^* is the effective capacitance of the system. It is convenient not to measure the nonlinear I–V characteristic directly but to measure the differential conductance $G = \mathrm{d}I/\mathrm{d}V$ as a function of the bias voltage V at a frequency of typically a few tens of Hz. The result is a temperature dependent bell shaped dip in conductance around zero bias (Fig. 12.29) which is due to the Coulomb blockade; it increases with decreasing temperature. In lowest order of $E_C/k_B T$ one finds for the differential conductance of a symmetric linear array of N uniform junctions in series [12.87–12.89]

$$G(V)/G_T = 1 - (E_C/k_B T)g(eV/Nk_B T), \tag{12.12}$$

With $E_C = e^2\ (N-1)/NC^*$; G_T is the asymptotic conductance at high voltage, and $g(x) = (x\sinh x – 4\sinh^2 x/2)/(8\sinh^4 x/2)$. The full width at half minimum of the conductance dip has in lowest order of $E_C/k_B T$ the universal value

$$V_{1/2} = 5.439 N k_B T/e, \tag{12.13}$$

which does not dependent on any device parameter (except the number N of junctions), and allows to determine T without calibration. Its measurement to determine T requires measuring a full conductance curve by sweeping the bias voltage, which will take a few minutes. In a faster mode, one can measure

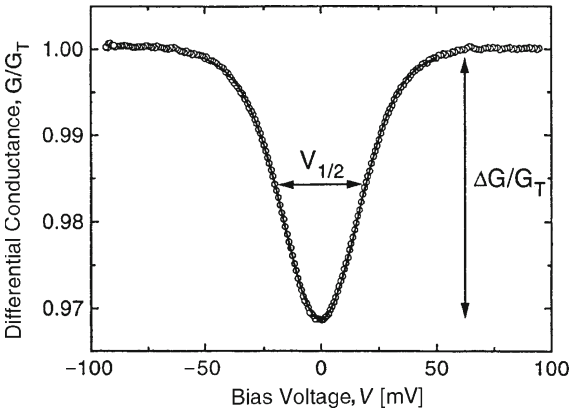

Fig. 12.29. Differential conductance G/G_{T} of a Coulomb blockade thermometer with $N = 20$ tunnel junctions at $T = 4.2\,\mathrm{K}$. The full line is the theoretical prediction (12.12). The two temperature dependent parameters $V_{1/2}$ prop. T (12.13) and $\Delta G/G_{\mathrm{T}}$ prop. T^{-1} (12.14) are indicated [12.88]

the depth of the dip, which is proportional to inverse temperature, and again in lowest order in $E_{\mathrm{C}}/k_{\mathrm{B}}T$, is given by

$$\Delta G/G_{\mathrm{T}} = E_{\mathrm{C}}/6k_{\mathrm{B}}T. \tag{12.14}$$

Equations (12.13) and (12.14) are the central results for a rather simple – requiring only a low-frequency resistance measurement – primary ($V_{1/2}$ with no adjustable parameter) or secondary ($\Delta G/G_{\mathrm{T}}$ with E_C as device parameter) thermometer. Introducing higher-order terms in $E_{\mathrm{C}}/k_{\mathrm{B}}T$ allows extending the range of operation of a CBT – which usually has a dynamic range of two decades in temperature – to lower T [12.87, 12.88].

A Coulomb blockade thermometer is a series of connected tunnel junctions biased at $+V/2$ and $-V/2$ at its two ends. Experiments have shown an excellent agreement between experimental data and theory, for example for the linear dependence of $V_{1/2}$ on temperature T (Fig. 12.30) or on the number N of tunnel junctions (Fig. 12.31) [12.87, 12.88]. Of course, one may have to take into account possible non-uniformities of the junctions. However, this influence is weak with changes in the I-V parameters of less than 1% if the areas of the junctions or their resistance vary by 10%, for example [12.87–12.89]. At low temperatures, a CBT can have an accuracy of 1% at 50 mK to 4 K, and 3% at 20 mK. The temperature ranges are limited by the finite height of the barrier as well as by the vanishing of the dip at high T (around 30–50 K). At low temperatures, the decoupling of the electrons from the lattice, the influence of background charges and possibly the approach to the full Coulomb blockade are the limiting factors [12.87–12.89].

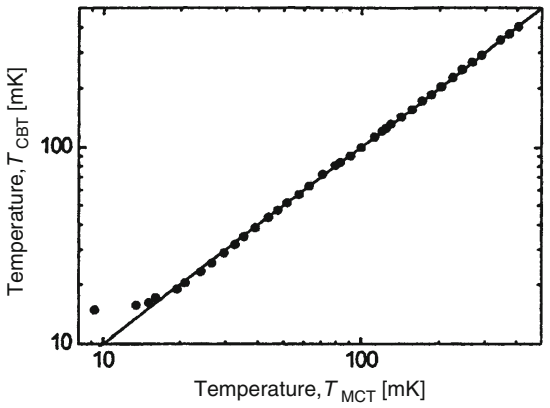

Fig. 12.30. Temperature T_{CBT} determined with a Coulomb blockade thermometer compared to the temperature determined with a ^{3}He melting curve thermometer. Saturation of the CBT values below 20 mK indicates the decoupling of the electrons from the phonons in the CBT [12.88, 12.89]

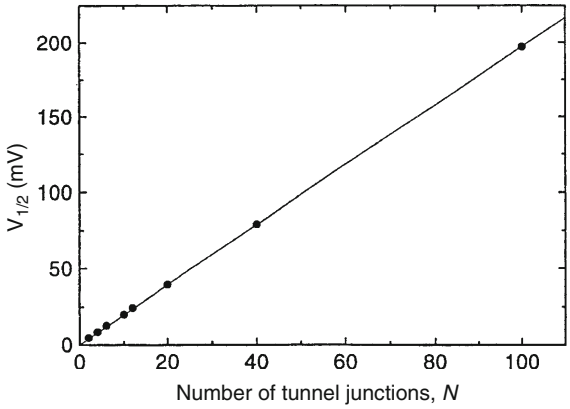

Fig. 12.31. Dependence of the full width $V_{1/2}$ at half minimum of the differential conductance of a Coulomb blockade thermometer (see Fig. 12.29) on the number of tunnel junctions of this thermometer at $T = 4.2$ K [12.88]

The problem of electron–phonon coupling at low temperatures seems to limit this thermometry device to $T > 10$ mK at present due to overheating the electrons by the measuring power (Fig. 12.30) (which is, of course, zero at zero bias) as well as by parasitic heat leaks. Actually, these devices are well suited to measure quantitatively the electron-phonon coupling at low temperatures [12.87, 12.89]. A CBT is insensitive to magnetic fields, because its operation is based on electrostatic properties. In [12.90], a sensor consisting of 100 tunnel junctions (100 nm normal conducting Al, Al_2O_3, 200 nm Cu) in

series with ten of them in parallel (total size $30\,\mu\mathrm{m}^2$, total resistance $300\,\mathrm{k}\Omega$) was shown to be insensitive to within 3% to magnetic fields up to 27 T at $T = 50\,\mathrm{mK}$. An earlier experiment with a similar device had shown no observable magnetic field dependence of the CBT reading to within 1% in fields up to 23 T at 0.42–1.46 K [12.90]. The precision was mainly limited by the high noise level of the resistive coil necessary to produce these high magnetic fields.

A review of the energy distribution of mesoscopic electron systems, and how it can be controlled, measured, and used in various micro- or nanostructured devices can be found in [12.87]. This reference as well as [12.91] gives detailed descriptions of the characteristics, of the device fabrication and on the instrumentation for CBTs. This instrumentation as well as the Coulomb blockade thermometers are available commercially.

12.7 Noise Thermometry

The conduction electrons in a metal perform random thermal movements (*Brownian motion*), which result in statistical voltage fluctuations of a resistive element. Therefore all resistive elements of an electronic circuit are noise sources. This noise is statistical, therefore we cannot make statements about its value at a fixed time, and the mean value of the noise voltage vanishes. However, we can calculate an effective time averaged mean square noise voltage

$$U_{\mathrm{rms}} = \sqrt{\langle u^2 \rangle_t}\,. \tag{12.15}$$

This noise voltage was investigated in 1928 by J.B. Johnson (*Johnson noise*) and H. Nyquist (*Nyquist theorem*). Nyquist arrived at the following equation for the component of the time averaged noise voltage within the frequency band from ν to $\nu + \mathrm{d}\nu$ of a resistor with value R at temperature T:

$$\langle u^2(\nu) \rangle_{\mathrm{t}} = 4 k_{\mathrm{B}} T R \, \mathrm{d}\nu\,, \tag{12.16}$$

valid for $\nu \ll k_{\mathrm{B}} T/h$.

If we measure within a frequency band of width $\Delta\nu$ we obtain

$$\langle u^2 \rangle = \int_{\nu}^{\nu+\Delta\nu} 4 k_{\mathrm{B}}\, T R \, \mathrm{d}\nu = 4 k_{\mathrm{B}}\, T R \Delta\nu\,. \tag{12.17}$$

This relation between noise voltage and resistance as well as temperature can be obtained by the following reasoning [12.92, 12.93]. If we connect two resistors – which act as noise sources providing random AC voltages of uncorrelated frequencies and phases – via lossless leads (Fig. 12.32), the power transported from R_1 to R_2 and vice versa is

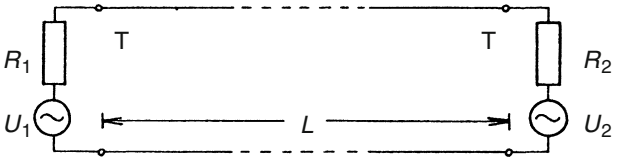

Fig. 12.32. Wiring to obtain the Nyquist theorem (see text)

$$\dot{Q}_{12} = R_2 I_1^2 = \frac{R_2 U_1^2}{(R_1 + R_2)^2}$$

and (12.18)

$$\dot{Q}_{21} = R_1 I_2^2 = \frac{R_1 U_2^2}{(R_1 + R_2)^2},$$

respectively. In thermal equilibrium $\langle \dot{Q}_{12} \rangle = \langle \dot{Q}_{21} \rangle$, and we have

$$\frac{\langle U_1^2 \rangle}{R_1} = \frac{\langle U_2^2 \rangle}{R_2}\,, \tag{12.19}$$

the R dependence of the noise voltage we were looking for.

To obtain the temperature dependence of the noise voltage we set the two resistances equal to each other, and join them by a connection with vanishing ohmic resistance but with an impedance $Z = R$. If we short the leads at time t, then the total transported energy at this time is trapped, and the enclosed wave train can be written as a sum of the eigenfrequencies of the transforming leads with length L,

$$\nu_n = \frac{nv}{2L} \tag{12.20}$$

with $n = 1, 2, \ldots$ and v being the transport velocity in the leads.

For large n, we can write

$$\mathrm{d}\nu = \frac{v\ \mathrm{d}n}{2L} \tag{12.21}$$

In thermal equilibrium at temperature T each mode has an electric and a magnetic degree of freedom with a mean energy $k_\mathrm{B}T/2$. Therefore the total energy in the interval $\mathrm{d}\nu$ is given by

$$\langle \mathrm{d}Q \rangle = 2\ \mathrm{d}n k_\mathrm{B} T/2 = 2k_\mathrm{B} T L\ \mathrm{d}\nu/v\,, \tag{12.22}$$

which is just the energy Q transported from R_1 to R_2, or vice versa, during the time $t = L/v$,

$$\langle \mathrm{d}\dot{Q}_{12} \rangle = \langle \mathrm{d}\dot{Q}_{21} \rangle = \langle \mathrm{d}Q \rangle / 2t = k_\mathrm{B} T\ \mathrm{d}\nu\,. \tag{12.23}$$

Therefore we have, with (12.18) and $R_1 = R_2$,

$$\langle u^2(\nu) \rangle = 4\dot{Q}R = 4k_\mathrm{B} T R\ \mathrm{d}\nu\,. \tag{12.24}$$

If we perform a quantum mechanical calculation, the result is the replacement of $k_B T/2$ (valid at $h\nu \ll k_B T$) by

$$\frac{h\nu/2}{\exp(h\nu/k_B T) - 1} \Rightarrow \frac{k_B T}{2} \quad \text{for} \quad h\nu \ll k_B T\,, \tag{12.25}$$

where the last requirement, $\nu/T \ll 20\,\text{GHz K}^{-1}$, is always fulfilled in practice. Equations (12.16, 12.17) are also obtained for this limit.

The experimental problems in using noise voltages for thermometry result mainly from the rather small size of the effect [12.3, 12.4, 12.10, 12.11, 12.92–12.97]. If we take, for example, $R = 1\,\text{k}\Omega$ and $\Delta\nu = 1\,\text{kHz}$, then

$$\text{at } 4\,\text{K}: \quad U_{\text{rms}} \simeq 10^{-8}\,\text{V},\ \dot{Q} \simeq 10^{-19}\,\text{W}, \tag{12.26}$$

and

$$\text{at } 10\,\text{mK}: \ U_{\text{rms}} \simeq 10^{-9}\,\text{V}, \dot{Q} \simeq 10^{-22}\,\text{W}. \tag{12.27}$$

At least the latter values are usually not measurable with semiconductor amplifiers and one has to use a SQUID with its extremely low intrinsic noise as the amplifying element. Two types of absolute noise thermometer have been used, which both measure the noise voltage by a resistor at the temperature T using a SQUID as a detector and amplifier.

In one method, the "resistive SQUID method", the resistor is directly connected to the Josephson tunneling junction(s) of the SQUID [12.10, 12.20, 12.94, 12.95]. Making use of the AC Josephson effect with a voltage across the junction, the SQUID serves as a very accurate voltage-to-frequency converter. The equation relating the voltage V to the Josephson frequency, $\nu_J = (2\,e/h)\,\text{V}$, contains only fundamental constants; the frequency is 484 MHz for a voltage of $1\,\mu\text{V}$. Thus, the noise voltage is measured by a frequency counter. The detector bandwidth $\Delta\nu$ is equal to $1/2\ \tau$ (τ: gate time of the frequency counter; in [12.95] for example, a time of 20 ms was chosen). Most importantly, the result is independent of circuit parameters like bandwidth or amplification factor, making it in principle a primary temperature technique. However, the oscillations are extremely small and special amplification and detection electronics is required. Further problems of this method, for example modification of the Johnson noise of the resistor by the Josephson junction and the impact of noise from external parts of the circuit, are discussed in [12.20, 12.94, 12.95]. Nonetheless, nowadays uncertainties as small as a few 0.1% at temperatures above 10 mK and 1% to about 1 mK can be obtained.

In the alternate technique, the "current sensing noise thermometer", the resistor is inductively coupled to the SQUID, which serves as a low-noise amplifier of the current generated by the thermal noise in the input coil (Fig. 12.33) [12.96, 12.97]. Analogous to (12.24), the mean square noise current flowing in the SQUID input coil per unit bandwidth $\Delta\nu$, arising from the thermal noise in the sensor, is given by

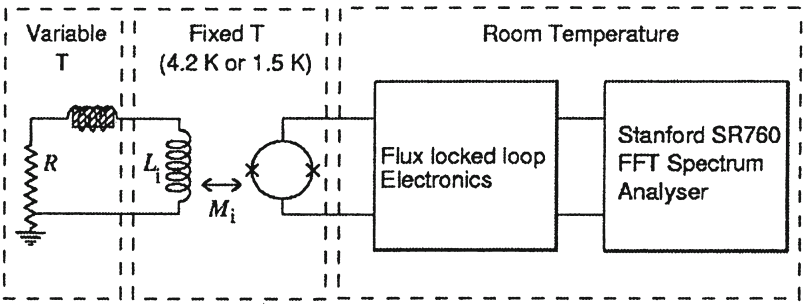

Fig. 12.33. Schematic diagram of the current sensing noise thermometer of [12.97]. One end of the noise resistor R is grounded to the thermal reservoir whose temperature is to be measured. The SQUID with its input coil L_i is held at a fixed temperature of 1.5 or 4.2 K for stability. A superconducting fixed-point device (see Sect. 11.4.3) can be incorporated into the SQUID input circuit, providing temperature fixed-points for calibration. Reprinted from [12.97], copyright (2003), with permission from Elsevier

$$\langle I^2 \rangle = [4k_\mathrm{B}T/R]\Delta\nu/[1 + (2\pi\nu\tau')^2], \tag{12.28}$$

with the time constant $\tau' = L/R$ determining the bandwidth, and L the total inductance of the input circuit. A rather small value R for the resistor, typically 0.1–1 mΩ, has to be chosen to match the circuit to the SQUID. In order to use this method in an absolute mode as a primary thermometer, a number of the parameters of the relevant circuit have to be measured independently.

In [12.96], all the required parameters of the circuit were measured or calculated, and the device was indeed used as a primary thermometer with an accuracy of 3% from 4 mK to 4 K. By the use of the SQUID as a low-noise amplifier, the device noise temperature was kept at 50 μK. Whereas in these early circuits for noise thermometry bulk resistive RF-SQUIDs with one Josephson junction were used as detectors and amplifiers, they were replaced in the more recent designs [12.97] of current noise-sensing thermometers by thin-film resistive DC-SQUIDs with two Josephson junctions. Their lower noise and higher sensitivity result in a higher accuracy and a shorter measuring time. The noise of the SQUID can be parameterized by the coupled energy equivalent sensitivity ε_c (for the definition see [12.97]) of the minimum detectable current in its input coil; it is around $500h$ (h: Planck's constant) for present commercial SQUIDs. This parameter ε_c determines the noise temperature

$$T_\mathrm{N} \approx \varepsilon_\mathrm{c}/2k_\mathrm{B}\tau' \tag{12.28a}$$

and the precision $\Delta T/T$ (see below).

The SQUID is used in a flux-locked loop mode. This design results in a significant improvement in speed and the possibility to use the circuit to measure much lower temperatures. Using a 0.34-mΩ Cu foil resistor, the equivalent amplifier noise temperature in the circuit of [12.97] was 8 μK in the frequency range of 0.5–1 kHz. Using their setup as a primary thermometer

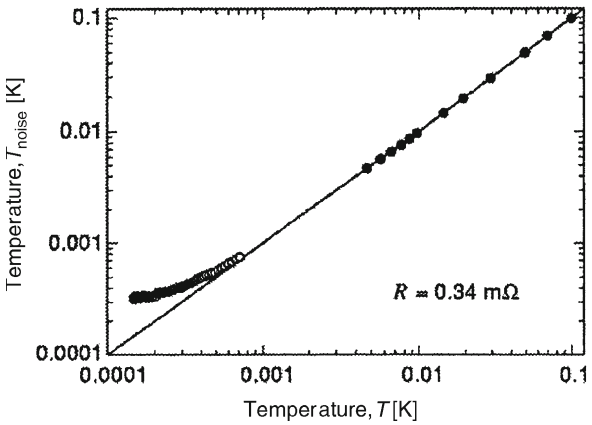

Fig. 12.34. Temperatures obtained from the current sensing noise thermometer of [12.97] vs. temperatures from a ^{3}He melting pressure thermometer (●) and a platinum NMR thermometer (○). At $T < 4.5$ mK, the noise thermometer reads hotter because of a heat leak into it. Reprinted from [12.97], copyright (2003), with permission from Elsevier

(by measuring the resistance value and SQUID gain) and fitting the measured frequency-dependent noise spectra to (12.28), the authors have achieved 1% agreement of the measured temperature with the temperature from the ITS-90 scale (Sect. 11.2) at 4.2 K. In a secondary mode, the device was calibrated at 100 mK and temperatures were measured from 4.2 K to below 1 mK. They agreed down to 4.5 mK to within 1% to temperatures obtained from a ^{3}He melting curve thermometer using the PLTS-2000 scale (Sect. 11.3). At lower temperatures, the temperatures from the noise thermometer were higher than those from a platinum NMR thermometer (Fig. 12.34), indicating a heat leak into the noise sensor. About 3.3 min of measuring time were required for 1.5% accuracy in temperature. With a higher resistance value, for example 5 mΩ, the noise temperature would increase to 30 μK, but 1% accuracy could be achieved in 10 s only.

Because of the stringent experimental requirements, noise thermometry will be used mostly by standards laboratories for calibration purposes while the experimenter will resort to some simpler means of thermometry. Indeed, noise thermometry has played an essential role in establishing the new temperature scale PLTS-2000 (Sect. 11.3). Very detailed investigations performed in this context have shown that the two main error sources of current noise thermometers seem to be parasitic noise from the measuring equipment, which adds to the noise from the thermometer, as well as heat leaking into the noise thermometer. The first problem can easily be taken into account in the analysis if it is temperature independent [12.10, 12.95].

To reduce the impact of parasitic heat input, a SQUID noise thermometer without any leads to the sample was recently used between 6 mK and

4 K [12.98, 12.99]. These authors used a superconducting pick-up coil wound around a high-purity Au sample as noise source. The coil is connected to the input coil of a DC-SQUID held at 1.2 K to form a superconducting flux transformer. The thermal motion of the conduction electrons in the Au sample cause fluctuations of the magnetic flux in the pick-up coil which are sensed by the SQUID. A resolution of 1% was achieved within 13 s.

In principle, a noise thermometer is a primary thermometer. In practice there are many severe experimental problems besides the small voltages, so that this method is not in wide use in research laboratories. Some of these problems are the following. All resistive elements of the electronic setup for noise thermometry are noise sources themselves. This situation has been improved by using a SQUID as a low-temperature amplifier. The remaining equipment is at temperatures between 4 K and 300 K and noise from the resonance circuit, for example, may affect the performance of the SQUID as well. Another important parameter is the effective bandwidth of the electronics and, last but not least, one has to determine the amplifying factor or gain of the total system. If noise thermometry is used as secondary thermometry, the system can be calibrated by putting the resistor at a known temperature. Another possibility is to build two identical electronic circuits and calibrate the two against each other, where one of them has the sensor as the noise source at unknown temperature and the other one has its sensor at a known temperature.

If we detect noise voltages, we are detecting statistical events, which have to be time averaged and, as for all statistical events, the accuracy depends on the measuring time t. If $t\Delta\nu \gg 1$, then the standard deviation for the temperature measurement via noise thermometry is given by

$$\Delta T/T = (\alpha\tau/t)^{1/2} \,. \tag{12.29}$$

with α a constant of order unity and depending on the method used. This means that the accuracy does not depend on temperature, which is an advantage if we want to apply this method at low temperatures.

12.8 Capacitance Thermometry

Capacitance measurements are as simple as resistance measurements and they usually have the advantage of negligible heating of the investigated samples. Actually these measurements can be performed with very high precision, in general much more accurately than a resistance measurement with comparable electronic effort. Therefore, if one has a material whose dielectric constant changes with temperature this will be a very attractive thermometric parameter to be measured in a capacitor. Indeed, some dielectric materials, in particular amorphous or glassy materials, show changes of their dielectric constant down to the lowest investigated temperatures [12.99–12.101]. Investigations by Frossati and coworkers [12.102, 12.103] of the low-frequency

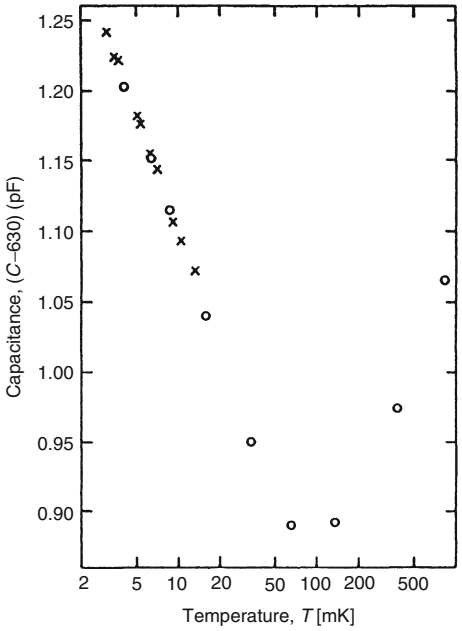

Fig. 12.35. Capacitance (−630 pF) of a capacitive glass thermometer (vitreous silica containing 0.12% OH^- ions) as a function of temperature. The data points were obtained at excitation frequencies of 1.0 and 4.7 kHz, at zero magnetic field (×) and at $B = 9\,\mathrm{T}$ (○) [12.103]

capacitance of a glass thermometer made from SiO_2 which contained about 1,200 ppm OH^- gave very encouraging results in the temperature range from 4 to 100 mK (Figs. 12.35 and 12.36). In particular, they showed that such a thermometer is field independent for fields up to 9 T (within 5%), and it has a time constant of order 1 s to the lowest investigated temperatures [the specific heat is typically 10 T (erg/g K), see Sect. 3.1.4]. In addition, heating effects are negligible, typically $< 10^{-12}$ W, because of the very small dielectric losses of vitreous silica, and because it is almost not affected by stray RF fields which limit the use of carbon resistors to $T > 5$ mK, for example (Sect. 12.5.2). The measurements can be performed with a commercial capacitance bridge or a bridge, as shown in Fig. 3.32 (with the inductances replaced by capacitors), see also the end of Sect. 13.1.

The dielectric constant ϵ of glasses (for example, Suprasil, Homosil, Spectrosil, BK 7, Kapton, smoky quartz [12.100–12.106]) as a function of temperature passes through a minimum whose position (at about 70 mK for 1 kHz) depends on frequency ν as $T_{\min} \underset{\sim}{\propto} \nu^{1/3}$ [12.102, 12.103]. At lower temperatures ϵ is independent of frequency for $h\nu \ll k_\mathrm{B}T$, with a slope $\mathrm{d}\ln\epsilon/\mathrm{d}\ln\ T \approx -10^{-4}$ (Fig. 12.35) and saturating at a few millikelvin (but see [12.106]). This temperature dependence of ε is, like the thermal and acoustic properties of glasses at low temperatures, explained by the tunneling

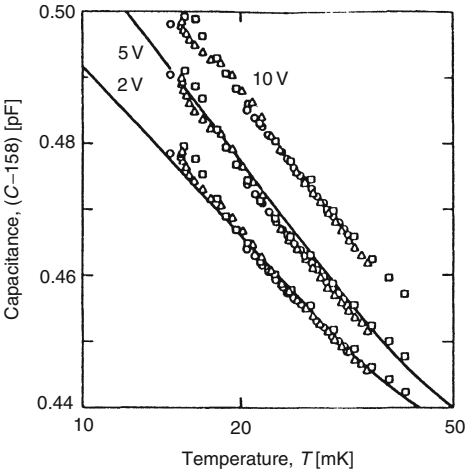

Fig. 12.36. Capacitance (−158 pF) of a capacitive glass thermometer as a function of temperature at the three indicated measuring voltages but all at the same frequency (4.7 kHz). The measurements were performed in magnetic fields of 0.0 T (○), 0.25 T (△), and 6.0 T (□) [12.102]

model [12.99–12.101]. The sensitivity $\mathrm{d}\ln\varepsilon/\mathrm{d}\ln T$ of Suprasil and Homosil glasses increases with their OH^- content for concentrations between 200 and 1,000 ppm, indicating that the OH^- dipoles dominate the dielectric behavior [12.104]. It was found that the dielectric constant depends also on the excitation voltage [12.102, 12.103, 12.105] (Fig. 12.36). Therefore these thermometers should be operated at constant voltage. The latter nuisance effect is influenced by the design of the glass thermometer (construction of electrodes, contacts, leads, etc.). Typical shapes of these thermometers are plates or tubes of 10–40 mm length and width, and some 0.1 mm thickness, covered with fired or sputtered noble metal electrodes, giving typical capacitances of 0.1–1 nF. The measurements are performed at some kilohertz and with voltages of 0.1 V to some volts applied to the electrodes, giving a sensitivity of about 10^{-4} pF at 100 pF and a temperature resolution of 0.1 μK at some millikelvins, even though the absolute changes of ϵ with T are small (Figs. 12.35 and 12.36). Unfortunately, the thermometers usually have to be recalibrated in each cooldown, mostly due to changing contributions from the leads. The recent result [12.107] that the velocity of sound and the internal friction of metallic and dielectric glasses change with temperature to at least 0.1 mK may make these thermometers suitable even for the microkelvin temperature range.

A capacitance thermometer based on the incommensurate crystal $(Pb_{0.45}Sn_{0.55})_2P_2Se$ has shown an order of magnitude higher sensitivity $\mathrm{d}\ln C/\mathrm{d}\ln T$ of about 5^*10^{-3} and a negligible field dependence for fields up to 20 T [12.108].

A rather simple, efficient and field-independent parallel plate capacitance thermometer has been developed by [12.109]. It consists of 17.8-μm-thick copper foils and 7.6-μm Kapton sheets glued together with a thin layer of Stycast 1266 and rolled into a tube. By choosing the foil and sheet dimensions appropriately, capacitances between 1 and 52 nF were achieved. The capacitors were investigated at 20 mK to 1.6 K (actually, they should be usable to room temperature) and at fields up to 18 T. The sensitivity is about 10^{-4} and the upper limit of the field dependence is 1% in temperature and 70 ppm in capacitance in the investigated temperature range up to 400 mK. Their frequency and voltage dependences are similar to those of other capacitance thermometers.

A suitable temperature dependence of ϵ down to 7 mK and the absence of a field dependence had been demonstrated earlier by Lawless and coworkers for $SrTiO_3$ glass–ceramic thermometers [12.110]; such thermometers are available commercially.

Capacitance thermometers with the negligible dependence of their dielectric constant on magnetic fields seem to be a very good choice for thermometry in high magnetic fields. However, the thermal coupling of a dielectric material whose capacitance is supposed to be measured and hysteresis effects have to be investigated; actually, most of the capacitance thermometers have to be recalibrated in each cooldown. In addition, the time-dependent heat release of non-crystalline solids (Sect. 10.5.3) has to be taken into account.

12.9 Magnetic Thermometry with Electronic Paramagnets

The magnetic thermometric method to be discussed in this section has been for a long time the conventional way to measure temperatures below 1 K. Its basis is the T^{-1} dependence of the magnetization

$$M = \frac{\lambda B}{\mu_0 T} \tag{12.30}$$

or of the susceptibility

$$\chi = \mu_0 M/B = \lambda/T \tag{12.31}$$

of a paramagnet with the Curie constant

$$\lambda = \frac{N_0 J(J+1)\mu_0 \mu_\mathrm{B}^2 g^2}{3k_\mathrm{B}} \,. \tag{12.32}$$

These equations are valid in the high-temperature approximation $\mu\mu_\mathrm{B}B \ll k_\mathrm{B}TJ$, where the susceptibility follows the Curie law. The above relations were deduced in Chaps. 9, 10 for non-interacting magnetic moments in an external magnetic field.

Due to the simple relation between the measured parameters χ or M and temperature, magnetic thermometry, in principle, is a primary method. However, again there are problems and deviations, making magnetic thermometry in practice a secondary method. The moments in paramagnetic dielectrics experience a local magnetic field B_{loc} which is different from the externally applied field B_{ex} and which has the following three components [12.3, 12.4, 12.111]:

$$B_{\mathrm{loc}} = B_{\mathrm{ex}} + B_{\mathrm{d}} + B_{\mathrm{w}} \,. \tag{12.33}$$

The demagnetization field B_{d} resulting from the magnetization of the paramagnet in a field is given for an ellipsoid magnetized in the direction of its symmetry axis by

$$B_{\mathrm{d}} = -f\mu_0 M/V \,. \tag{12.34}$$

The geometry factor f can be calculated for various ratios of length to diameter of an ellipsoidal sample

l/d :	1	1.5	2	3	4	5	6	∞
f :	0.333	0.233	0.174	0.108	0.075	0.056	0.043	0

These effects are of great importance, of course, for superconductors (which are ideal diamagnets) as well as for ferromagnets; they can be quite appreciable for paramagnets as well.

The Weiss field B_{w} results from the neighbouring partially aligned dipoles and is

$$B_{\mathrm{w}} = \alpha\mu_0 M/V \,. \tag{12.35}$$

The parameter α depends on the symmetry of the crystal; for a cubic crystal $\alpha = 1/3$. We then have

$$B_{\mathrm{loc}} = B_{\mathrm{ex}} - (f - \alpha)\mu_0 M/V \,. \tag{12.36}$$

The local susceptibility

$$\chi_{\mathrm{loc}} = \mu_0 M/B_{\mathrm{loc}} = \lambda/T \tag{12.37}$$

follows the Curie law. Actually we are measuring

$$\chi = \mu_0 M/B_{\mathrm{ex}} \,, \tag{12.38}$$

which leads to

$$\chi = \chi_0 + \frac{\lambda}{T - (\alpha - f)\lambda/V} = \chi_0 + \frac{\lambda}{T - \Delta} \,, \tag{12.39}$$

where a (hopefully temperature independent) background contribution χ_0 resulting from other parts of the experimental setup – besides the thermometric sample – has been included. The latter relation (without the first term) is known as the Curie–Weiss law. The Weiss constant Δ depends on the shape of the sample, the symmetry of the crystal, and the interactions between the

moments. It can be small or may even vanish for a sphere of a crystal with cubic symmetry, where $B_{\mathrm{loc}} = B_{\mathrm{ex}}$. In addition, of course, it is small for small Curie constants λ. Because of the usually unknown parameters in (12.39), we have to calibrate our thermometer at several temperatures, making it a secondary thermometer. This calibration can be performed against the ^{3}He vapour pressure at $T \geq 0.4\,\mathrm{K}$, against a superconducting fixed point device or the ^{3}He melting pressure at $T \leq 0.3\,\mathrm{K}$, etc.

Substances suitable for electronic magnetic thermometry are paramagnets containing elements with partly filled 3d or 4f electronic shells. As mentioned in Chap. 9, the paramagnetic salt with the lowest ordering temperature is CMN with $T_{\mathrm{c}} \simeq 2\,\mathrm{mK}$. This value can be further reduced by partly replacing the magnetic Ce^{3+} ions in CMN by non-magnetic La^{3+} ions, possibly to $T_{\mathrm{c}} \leq 0.2\,\mathrm{mK}$ if only 5% or less cerium remains [12.112–12.115]. These salts can be used over the widest temperature range known and indeed it is the most widely applied paramagnetic thermometer [12.3, 12.4, 12.7, 12.8, 12.10, 12.20, 12.25,12.96,12.111–12.121]. It has also played an important role in establishing the new low-temperature scale PLTS-2000 (see Sect. 11.3). A CMN single crystal is a nearly perfect paramagnet if the temperature is not too low, say for $T > 5\,\mathrm{mK}$. The use of a single-crystal sphere is, of course, inconvenient. Therefore, in most cases powders compressed to a cylindrical shape have been used. However, its thermal conductivity is low and it is difficult to make thermal contact to it. Hence, usually a mixture of CMN powder plus grease (or another suitable liquid) has been compressed together with a brush of fine metal wires (Fig. 12.37). Thermal contact is then made via these wires. Of course, if the temperature of liquid ^{3}He is to be measured, CMN powder can be immersed in the liquid itself (Fig. 12.37), taking advantage of the low thermal boundary resistance between these two materials (Sect. 4.3.2). Many groups have used such a thermometer in the shape of a cylinder with its diameter equal to its length to keep deviations from the Curie law small and to make their temperature scales comparable [12.20,12.116,12.117,12.121]. It has been

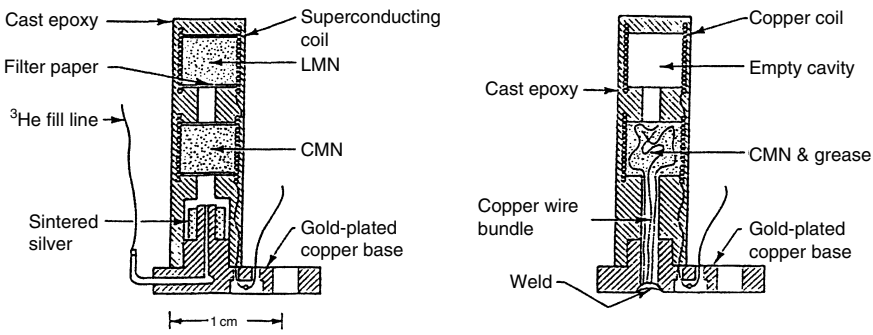

Fig. 12.37. Schematic of setups for paramagnetic thermometry with paramagnets such as CMN; for details see text [12.25]

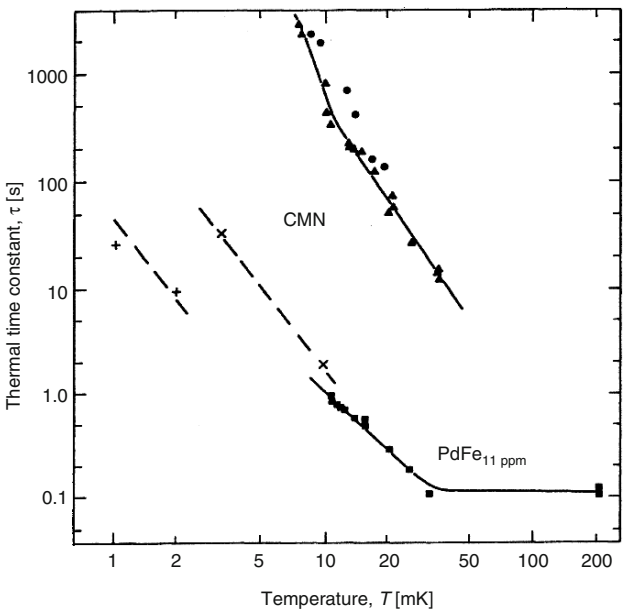

Fig. 12.38. Thermal time constant of the indicated paramagnetic thermometers. The data (+, ×, ●, ▲) for CMN are from [12.25, 12.118, 12.120], respectively. The PdFe data are from [12.120]

found that the Weiss constant $|\Delta|$ is in the range of several 0.1 mK and that such a CMN thermometer can follow the thermodynamic temperature scale to 3 mK to with in about 0.2 mK, but a more typical limit is 5–8 mK. The thermal time constant of such thermometers still is of order 10 (10^3) s at 40 (10) mK (Fig. 12.38) [12.25, 12.118, 12.120]. This has recently been improved by a design described in [12.118], see Fig. 12.39. This thermometer follows a Curie–Weiss law between 7 and 250 mK with $\Delta = -0.004$ mK. To obtain a resolution of 10^{-4} at 8 mK, a drive level in a bridge of the design shown in Fig. 3.32 was necessary which gave a heating of 10 pW (probably mostly eddy currents in the Ag). Most important, this CMN thermometer has a time constant of only 10 s at 2 mK (Fig. 12.38). With a modified fitting equation, it has been used to 1 mK, and, with the Ce^{3+} ions partly replaced by La^{3+} ions, even to 0.4 mK. With the improvement of measuring techniques the use of salts with larger Curie constants than CMN – and correspondingly higher ordering temperatures [12.3, 12.4, 12.7] – does not seem to be warranted anymore, so CMN seems to remain unrivalled among the salts. This has been confirmed by the recent results of [12.20], where resolution and reproducibility of about 10^{-4} have been obtained between 0.5 and 3 K for a CMN powder thermometer.

To avoid the thermal equilibrium and chemical stability problems, in particular dehydration, (at 25°C the water vapour pressure of CMN corresponds to 25% humidity) encountered when paramagnetic salts are employed for

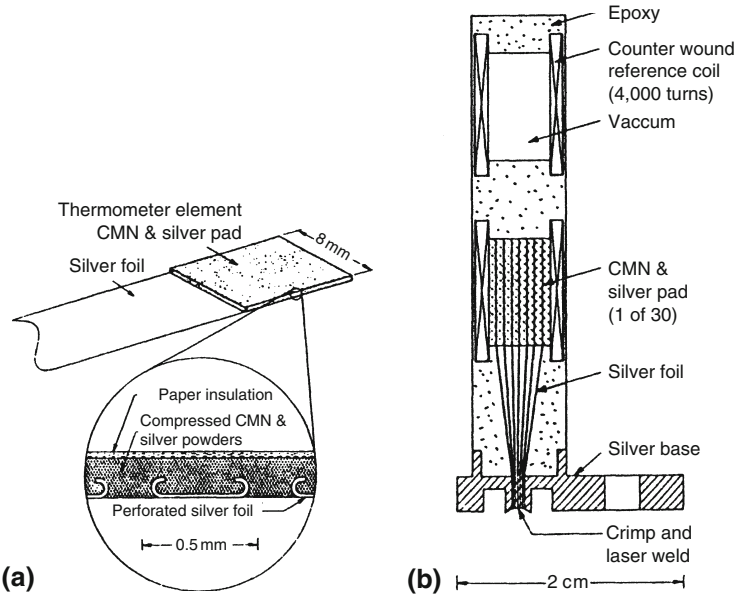

Fig. 12.39. Single element (**a**) and completed design (**b**) of the CMN thermometer of [12.118]

thermometry, various dilute paramagnetic *alloys* have been used for magnetic thermometry. These metallic alloys have a reasonably good thermal conductivity, and it is easy to make thermal contact to them. An example is Cu with some ppm of Mn [12.122]. With such a sample, 1% accuracy in a field of 0.1 mT at 5 mK can be obtained using a SQUID as the detecting element.

At the University of Bayreuth, we have very successfully used *Pd*Fe alloys with Fe concentrations of the order of 5–30 at ppm [12.38, 12.120, 12.123]. If one buys "pure" Pd of 4 N (or 5 N) purity it usually contains just the right concentration of Fe impurities. In these alloys, the Fe and its Pd surroundings have a "giant" magnetic moment of $14\,\mu_B$, giving a rather large signal. Spin glass freezing of these moments occurs at T_f (mK) $\simeq 0.1 x_{Fe}$ (ppm) (where x_{Fe} is the concentration of Fe in ppm) [12.38], and the susceptibility follows a T^{-1} dependence to quite low temperatures (Figs. 12.40 and 12.57); the data indicate that $|\Delta| < 0.2$ mK. The accuracy of the calibration is better than 1%, and the sensitivity is about 10^{-4} at 10 mK and 10^{-3} at 100 mK, comparable to CMN thermometers. The very simple design of such a thermometer is shown in Fig. 12.41. Due to its good thermal conductivity and ease of making thermal contact, such a thermometer has a rather short time constant of at most 1 (0.1) s at temperatures above 10 (30) mK (Fig. 12.38). Such a PdFe thermometer calibrated with an NBS superconducting fixed-point device (Sect. 11.4.2) is our standard thermometric method for the temperature range between about 5 and 500 mK. The only drawback of a PdFe thermometer is

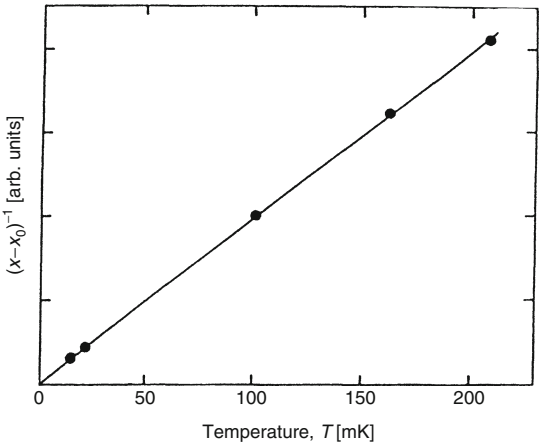

Fig. 12.40. Reciprocal of the susceptibility χ minus a background susceptibility χ_0 of a *Pd*Fe sample containing 15 ppm Fe as a function of temperature. The temperatures for calibration of the susceptibility thermometer are obtained from a superconducting fixed-point device such as the one shown in Fig. 11.1 [12.120]

its sensitivity to magnetic fields (it has to be shielded from stray fields, but the earth's field is okay, therefore one can use a superconducting shield) [12.38].

Another paramagnetic metallic spin glass very suitable for susceptibility thermometry is $Au\mathrm{Er}^{+}$ [12.124]. Because of the weaker exchange interaction between Er ions in Au compared to Fe in Pd, Er concentrations of several 100 ppm can be used without the magnetization showing significant deviations from the Curie–Weiss law. For example, the AC susceptibility χ of an Au sample containing 660 pm Er follows this law to about 1 K [12.124]. The ratio of the temperature at the maximum of χ to the content of Er^{+} ions (1.4 μK/ppm) is about three orders of magnitude lower than for Fe^{3+} impurities in Cu (1 mK/ppm). In the setup shown in Fig. 3.28, this thermometer has been used for thermal conductivity measurements to 6 mK.

High-resolution magnetic thermometers using paramagnetic salts, in particular for the investigation of critical phenomena like heat capacity and thermal conductivity at the very sharp lambda transition of liquid ^{4}He, have been developed by the groups of Lipa et al. [12.125–12.127], (Fig. 12.42) and then Ahlers et al. [12.128]. Both groups have used copper ammonium bromide ($\mathrm{Cu(NH_4)_2Br_4\ 2H_2O}$) either directly in liquid helium or grown onto a matrix of Cu wires for thermal contact. The salt is used at temperatures closely above its magnetic ordering transition at 1.83 K, where the susceptibility changes strongly with temperature. This change induces a persistent current in a superconducting coil wound around the sample. The current is transferred by a superconducting flux transformer to an RF-SQUID and amplified for readout. Typical sensitivities are between 0.3 and 1 $\mu\mathrm{K}/\Phi_o$(Φ_o: flux quantum) in a field of 10 mT near the Curie temperature of the salt. With a resolution of

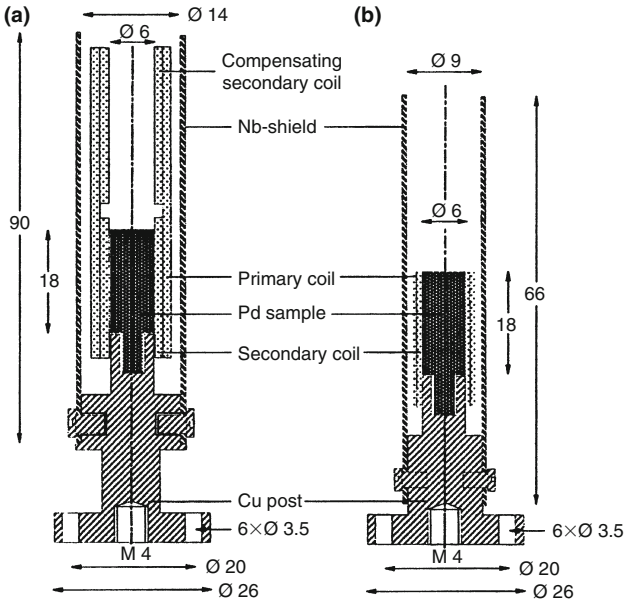

Fig. 12.41. Design of *Pd*Fe susceptibility thermometers. (**a**) With compensated secondary coils; (**b**) without compensated secondary coils. Dimensions are given in mm. The sample is a palladium rod containing 10–30 ppm Fe. Slits should be cut into the Pd rod to reduce eddy-current heating. If the susceptibility is measured with a SQUID then the primary coil may contain two layers of 0.1 mm Cu-cladded NbTi wire and the secondary coil ten layers of 25 µm Cu wire. If the susceptibility is measured with a mutual inductance bridge the number of windings should be increased, e.g., to 400 and 10^4, respectively. The two coils can be wound directly onto each other. The sample is protected against magnetic fields by a superconducting Nb shield

10^{-4} Φ_o of the SQUID this then results in sub-nanokelvin temperature resolution (Fig. 2.10b), a noise level of $3 \times 10^{-10}\,\mathrm{K}/\sqrt{\mathrm{Hz}}$, and drift rates of less than $0.1\,\mathrm{nK\,h^{-1}}$ [12.125–12.127]. Of course, to achieve these results requires a careful design with a very stable control of the temperature of four thermal control stages in series with the calorimeter as well as an effective magnetic shielding of thermometers and leads to the SQUID.

Using salts with Curie temperatures in other temperature ranges, this type of thermometer may be used there. For example, the miniature susceptibility thermometer of [12.129] using $\mathrm{La}_x\mathrm{Gd}_{1-x}\mathrm{Cl}_3$ with different x to adjust the Curie temperature to the desired temperature range ($T_\mathrm{c} = 2.2\,\mathrm{K}$ for $x = 0$) has achieved a resolution of 0.2 nK in a 1-Hz bandwidth, a drift rate of less than $0.2\,\mathrm{nK\,h^{-1}}$ at 2.2 K, and a time constant of 30 ms.

A high-resolution magnetic thermometer using the giant-magnetic-moment alloys PdMn_x (or PdFe_x) has been described in [12.130]; again, the Curie temperature can be adjusted by changing x, for example to 1.5–3 K

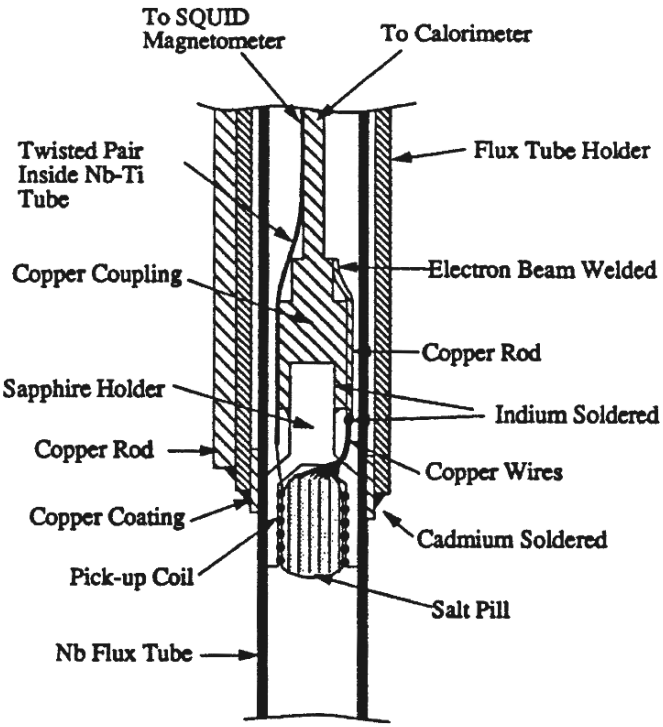

Fig. 12.42. High-resolution paramagnetic susceptibility thermometer used in [12.125–12.127] for measurements of the heat capacity of liquid ^{4}He very close to its superfluid transition temperature (see Fig. 2.10)

for $x = 0.6$–0.9 at.% Mn. The advantages of this metal compared to the salts are its inertness and that thermal contact can be easily established. The authors also use a SQUID magnetometer for detection of the signal and have achieved comparable resolution, noise level, and drift rates. For experiments with very limited space, the group has used sputtered films of $PdFe_{0.68\,at.\%}$ with somewhat less resolution [12.131].

The lower limit for a paramagnetic thermometer is given by the deviation of χ from a Curie–Weiss law. The upper limit of the thermometer's temperature range is governed by the loss in sensitivity due to $\chi \propto T^{-1}$, which is usually at about 1 K, depending on the material and on the electronic equipment.

Examples of typical electronic setups for measuring electronic susceptibilities of paramagnets suitable for thermometry are shown and discussed in Sect. 3.4.2.

Magnetic thermometry has the advantages that it is based on a simple and quick measurement, one can have a rather large sensitivity of typically 10^{-4}, there is essentially no heating due to the measurement, one has a simple

T–χ relation (therefore calibration is easy), and the thermometer can be homemade. Another advantage of magnetic thermometry for low-temperature physics is the increase of its sensitivity with decreasing temperature. If well designed, such a thermometer will have a rather short thermal response time of a few seconds at 10 mK.

12.10 Magnetic Thermometry with Nuclear Paramagnets

The low-temperature limit of magnetic thermometry is given by the ordering temperature of the magnetic moments; for electronic magnetic moments this is about 1 mK for the CMN and PdFe thermometers discussed earlier. With the extension of the accessible temperature range to lower and lower temperatures thermometric methods for lower and lower temperatures have to be invented. To extend magnetic thermometry to temperatures below a few mK one has to switch from electronic paramagnets to nuclear paramagnets. The change to the much smaller nuclear magnetic moments allows the use of magnetic thermometry to at least the low microkelvin temperature range. Due to the small nuclear magnetic moments we now have a much smaller susceptibility and therefore much smaller signal, requiring more sensitive detection methods; these are SQUID or resonance techniques [12.132–12.136], which will be described in this section. In addition to the extension of the temperature range, we can now switch to pure metals with their good thermal conductivity and contact and fast nuclear spin–lattice relaxation, resulting in fast thermal response times – as we did when going from electronic magnetic refrigeration to nuclear magnetic refrigeration.

The parameter to be measured is the nuclear susceptibility

$$\chi_\mathrm{n} = \lambda_\mathrm{n}/T_\mathrm{n} \quad \text{(Curie law)} \tag{12.40}$$

with the Curie constant

$$\lambda_\mathrm{n} = \frac{N_0 I(I+1)\mu_0 \mu_\mathrm{n}^2 g_\mathrm{n}^2}{3k_\mathrm{B}} \,. \tag{12.41}$$

These equations are valid in the "high-temperature limit" $g_\mathrm{n}\mu_\mathrm{n}\,\mathrm{B} \ll k_\mathrm{B}T$, where the nuclear magnetic dipoles can be treated as non-interacting.

In many metals this nuclear Curie law should be valid to at least a few microkelvin (or possibly even 0.1 μK). This seems to be true for Cu and Pt to within about 1% in fields of less than 1 mT (see Sect. 10.1 and Figs. 10.4 and 10.5) [12.137]. However, recently deviations have been observed for the intermetallic compound $AuIn_2$ [12.138] and for Tl [12.139], for example, already at about 100 μK in fields of some millitesla, therefore some caution may be appropriate when new materials are introduced for thermometry.

Requirements for the validity of the nuclear Curie law are the absence of changing internal fields due to nuclear magnetic or electronic magnetic ordering in the relevant temperature range, and the absence of nuclear electric quadrupole interactions (which means cubic lattice symmetry or, better, $I = 1/2$; see Sect. 10.6).[1] In addition, we need a short τ_1 (because we are measuring nuclear spin temperatures T_n but are usually interested in the electronic temperature T_e or in the equilibrium temperature of the material) and the absence of a superconducting transition. Nuclear magnetic thermometry dominates the low- and the sub-millikelvin temperature range but at higher temperatures the signals can become rather weak and may be dominated by contributions from electronic magnetic impurities. Therefore an adequate measuring technique – mostly a resonance method – is of utmost importance.

12.10.1 Non-Resonant, Integral Detection of Nuclear Magnetization

Of course, we can directly measure M_n or χ_n statically as we do in electronic magnetic thermometry. However, now due to the small nuclear moment necessarily we need a SQUID as detector with its high sensitivity to measure nuclear magnetization. In the experiment whose results are shown in Fig. 12.43 [12.141], the magnetization of a 6 N pure Cu sample in a field of 0.25 mT was investigated with a sensitivity of 10^{-3} flux quanta ϕ_0 ($\phi_0 = 2 \times 10^{-8}\,\mathrm{mT\,cm^2}$), resulting in $\Delta T/T = 5 \times 10^{-4}$ or 5 μK at 10 mK in a field of 1 mT. The result gave agreement with the calculated nuclear Curie constant of Cu and $M_n \propto 1/T$ in the investigated temperature range even up to 0.9 K! However, in general, one measures a combination of nuclear and electronic magnetizations $M_n(T) + M(T)$ in a direct, non-resonant measurement, and then 1 ppm Fe or Mn in Cu would give the same signal as the 100% Cu nuclei. As shown by Hirschkoff et al. [12.142, 12.143], electronic contributions from the wire of the primary or secondary coils or from the insulation already may cause serious problems. These problems can mostly be eliminated by measuring in a magnetic field large enough to saturate the large electronic moments at the temperatures involved (also at the calibration points!), which, for example, is $B/T \geq 1\,\mathrm{T\,K^{-1}}$ for 3d elements in the cubic intermetallic compound $AuIn_2$ (Fig. 12.44) [12.144]. In this latter work a simpler but much less sensitive commercial fluxgate magnetometer was used instead of a SQUID in the temperature range 15–500 mK. If the electronic moments are saturated, they only give a temperature-independent background to the signal. Of course, there is the possibility of other background contributions from the sample holder, coils, etc. which may give temperature-independent as well as temperature-dependent contributions. The direct method has experimental problems but, unlike the following methods, it does not lead to heating of the sample due to the measuring process.

[1] This, of course, does not apply if "nuclear quadrupole resonance" is applied for thermometry, as proposed for very low temperatures in [12.140].

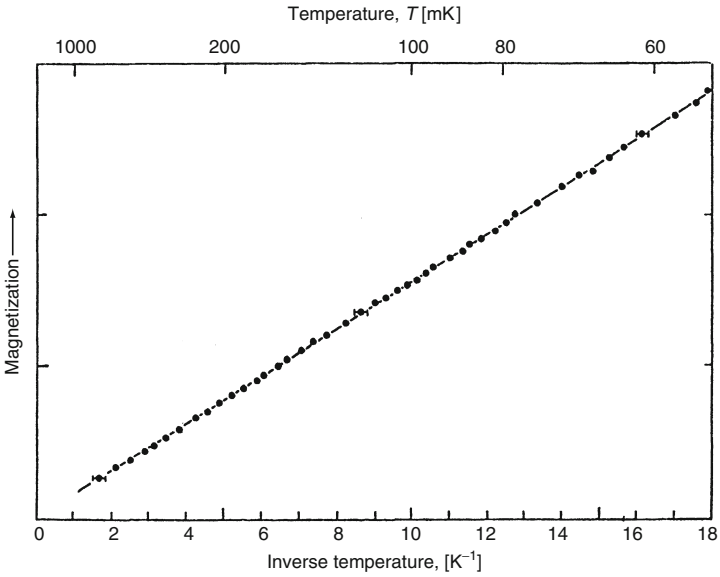

Fig. 12.43. Temperature dependence of nuclear magnetization of copper as a function of inverse temperature (the temperature scale is shown on the top horizontal axis). The static nuclear magnetization of Cu in a field of 0.25 mT was measured with a SQUID. The temperatures were deduced from the ^{3}He melting pressures [12.141]

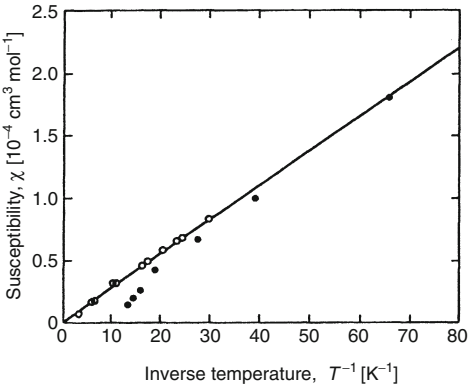

Fig. 12.44. Molar nuclear susceptibility of $AuIn_2$ in different magnetic fields plotted against T^{-1}. The measuring fields are 20 mT (●), 193 and 640 mT (○), respectively. The last two magnetic fields are strong enough to saturate the electronic moments, so that only the changes in nuclear susceptibility are measured (data from [12.144])

12.10.2 Selective Excitation but Non-Resonant Detection of Nuclear Magnetization

A variation of the method discussed earlier, avoiding the problem of background contributions, is the resonant, selective destruction of the nuclear polarization in an external field B_z by irradiating the sample with an RF field at resonance. The frequency of the RF field has to be in resonance with the Zeeman splitting

$$h\nu = \mu\mu_{\mathrm{n}} B_z / I \,. \tag{12.42}$$

It has to be perpendicular to the polarizing static field B_z, so it can induce transitions from the lower to the upper nuclear levels. In this way the static magnetization of the nuclei is changed and this change can be detected with a SQUID (Fig. 12.45) [12.145, 12.146]. The method combines the high sensitivity of the SQUID with the selectivity of resonant excitation; electronic contributions or contributions from other nuclei are not detected because they are not in resonance. Some results for "SQUID NMR" on Cu are shown in Fig. 12.46. The destroyed nuclear magnetization recovers with the spin–lattice relaxation time τ_1. This method is often applied when the more conventional NMR techniques to be discussed later are inappropriate; for example, for very broad resonances, experiments at very low frequencies [12.147,12.148] or when heating effects are a problem. A disadvantage of this method is that a change of magnetization of all the materials within the SQUID sensing volume will lead to changes in the baseline of the signal (Fig. 12.46).

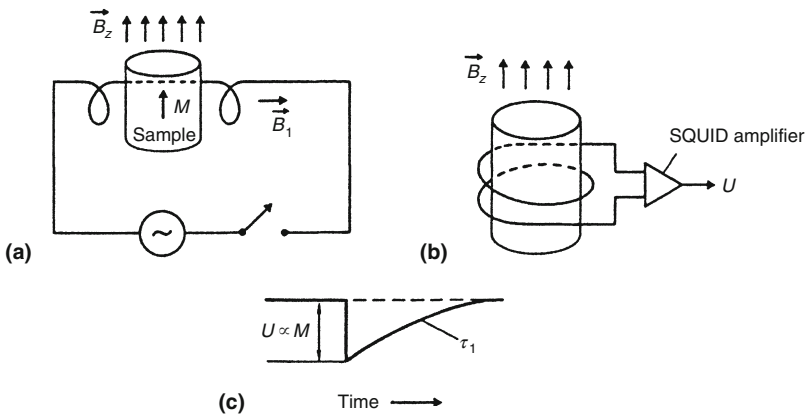

Fig. 12.45. Schematic for the technique of SQUID NMR thermometry. (**a**) The magnetization of the sample induced by the static field B_z is destroyed by applying a RF pulse of strength B_1 at the resonance frequency. (**b**) The resulting change of the magnetization is detected by a SQUID amplifier. (**c**) The voltage U detected by the amplifier – which is proportional to the magnetization M – changes with time when the magnetization recovers with the spin lattice relaxation time τ_1

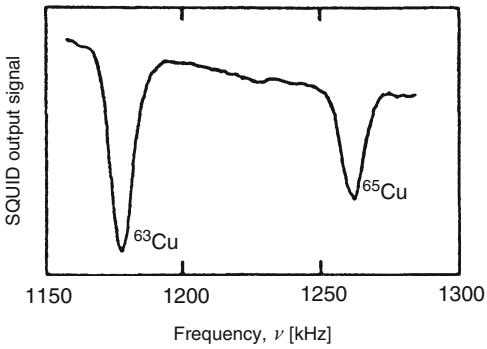

Fig. 12.46. A SQUID NMR spectrum of Cu taken at a sweep rate of $15\,\mathrm{kHz\,s^{-1}}$ at 0.65 K in $B_0 = 104\,\mathrm{mT}$. The vertical signal represents the total nuclear magnetization of the specimen which is reduced when the frequency is swept through the resonance of the two Cu isotopes [12.145]

The method of low-frequency pulsed SQUID NMR [12.147–12.149] has been substantially improved by using very sensitive commercial DC-SQUIDs as first-stage, low-noise preamplifier. They have a coupled energy equivalent sensitivity of the minimum detectable current in the input coil of the SQUID of a few $100h$ at a bandwidth of 3.4 MHz, (h: Planck's constant) [12.150–12.152]. In these spectrometers, the superconducting NMR receiver coil around the sample together with the input coil of the SQUID form a flux transformer circuit; their inductances should be similar to optimize the coupled flux. A changing magnetic flux in the receiver coil due to the precessing magnetization of the sample after applying an NMR pulse results in a current in the SQUID input coil to maintain a constant flux in the superconducting loop. The RF input circuit, which is contained in superconducting shields in order to reduce noise from extraneous magnetic fields, can either be broadband [12.147, 12.148, 12.150, 12.151, 12.153] or tuned [12.149, 12.150, 12.152]. For field stability, the static field can be trapped in a superconducting niobium cylinder. The noise temperature of the system is about 0.1 K, much better than for a typical cooled semiconductor preamplifier. The signal from the SQUID can be directly coupled to the room temperature amplifier without deterioration in noise performance.

In the broadband mode with bandwidth of about 3 MHz at Larmor frequencies of up to 500 kHz [12.150, 12.151], the SQUID was operated in a flux-locked loop with additional positive feedback to enhance the dynamic range, to improve gain stability, and giving a short recovery time of order $10\,\mu\mathrm{s}$; this allows investigations of samples with short spin-spin relaxation times. A substantial advantage is the possibility of changing the NMR frequency without changing the detection electronics. Experimental results obtained with such a system are shown in Fig. 12.47. Similar broadband, low-noise SQUID NMR setups have been described in [12.153].

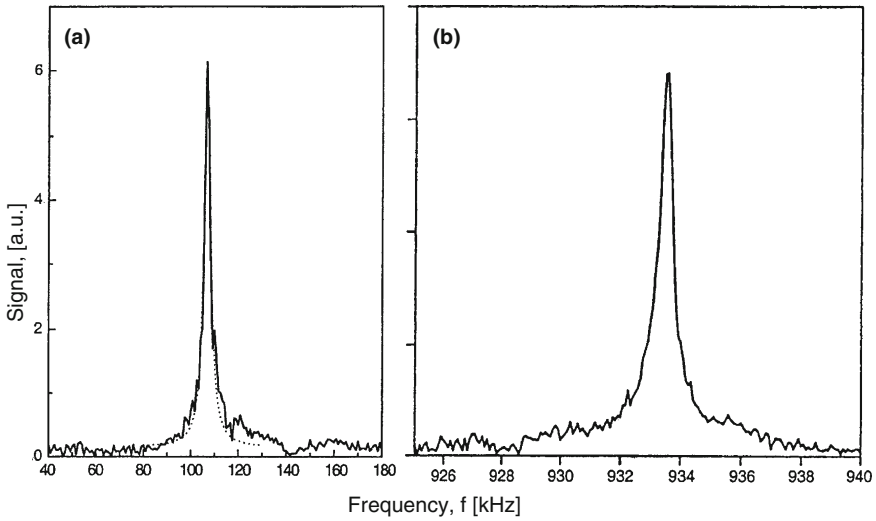

Fig. 12.47. Fast-Fourier transforms of free-induction decay signals obtained by SQUID NMR in: (**a**) a broadband circuit for 6×10^{19} ^{195}Pt nuclear spins in a single crystal of UPt_3 in the superconducting mixed phase at 40 mK [12.151], as well as in: (**b**) a tuned circuit for 5×10^{18} ^{3}He nuclear spins at 4.2 K. Reprinted from [12.151] and [12.152], respectively, copyright (2000), with permission from Elsevier

As discussed in [12.150,12.152], a tuned input circuit gives a higher signal-to-noise ratio at higher frequencies, above a few 100 kHz. In this mode, the pick-up coil and the SQUID input coil form part of a resonant circuit at around 1 MHz, with a noise of order 0.1 K. Here the receiver coil is made from normal conducting wire. Such a system has been used in particular to investigate very small numbers of spins, for example 10^{18} spins in thin ^{3}He films, or when the RF-penetration is limited to the skin depth in well-conducting metallic samples (Fig. 12.47).

12.10.3 Resonant Excitation and Resonant Detection of Nuclear Magnetization

The most commonly used method in nuclear magnetic thermometry are Nuclear Magnetic Resonance (NMR) techniques which avoid electronic or any other non-resonant contributions. There are two ways to do nuclear magnetic resonance: in the continuous wave mode or with pulses. Excellent books describe these very important methods which are not only of relevance for thermometry but have found many applications in physics, chemistry, biology, and medicine. I cannot discuss these methods in as much detail as their importance would require but refer to relevant books and review articles (see, e.g., [12.3, 12.4, 12.7, 12.132–12.136]).

Continuous Wave Nuclear Magnetic Resonance

For continuous wave NMR (CW NMR) [12.132–12.135,12.154,12.155] we consider a sample whose nuclear moments are magnetized by a static field B_z in the coil of a resonance circuit. The sample changes the inductance of the coil by the factor $(1 + \chi_n)$. When the static magnetic field applied to the sample is swept through the nuclear magnetic resonance, transitions between the nuclear energy levels are induced by an RF field

$$B_y = B_1 \sin(\omega t) \tag{12.43}$$

applied perpendicular to the static field. The necessary energy is taken from the resonance circuit, resulting in a decrease of its quality factor. Assuming that the line shape at resonance is temperature independent, the amplitude of the signal is proportional to χ_n and therefore to T_n^{-1}. The electronics for this method is shown in Fig. 12.48. One has to use small RF power to keep eddy-current heating small [12.156] and to avoid disturbing or heating the nuclear spin system from thermal equilibrium; therefore the signals are rather small. To increase the sensitivity, very often the frequency or the magnetic field is modulated at audio frequencies and the signal is detected with lock-in techniques.

It can be shown that the signal at resonance, $\omega = \omega_0$, in CW NMR is proportional to the imaginary part of the dynamic nuclear susceptibility

$$\chi_n(\omega_0) = \chi'_n - i\chi''_n , \tag{12.44}$$

with

$$\chi''_n(\omega_0) = \frac{\omega_0 \tau_2^*}{2} = \frac{\chi(0) B_z}{\Delta B_z} \propto 1/T_n , \tag{12.45}$$

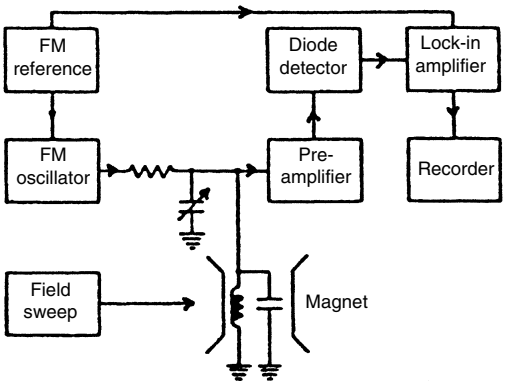

Fig. 12.48. Block diagram of the electronics used by Corruccini et al. [12.155] for CW NMR. The cw oscillator is frequency modulated at 100 Hz as the magnetic field is swept through the resonance of the sample inside of the coil of the resonance circuit

in the case that the signal is not saturated; here ΔB_z is the resonance width at half maximum. Hence the dynamic susceptibility is enhanced with respect to the static one by the ratio $B_z/\Delta B_z$ which can be of order 10^2–10^3 for Cu or Pt, for example.

Pulsed Nuclear Magnetic Resonance

In the today mostly used pulsed nuclear magnetic resonance technique [12.132–12.136, 12.157–12.161], again a static field B_z keeps a nuclear magnetization M_n in the z-direction. But now we apply perpendicular, in the y-direction, a short pulse of a sinusoidal field $B_y = B_1 \sin(\omega t)$ at the resonance frequency given by (12.42). This RF pulse tips the nuclear magnetization by an angle

$$\theta = \pi B_1 / B_z \tag{12.46}$$

away from the z-direction. The magnetization M_n then precesses around B_z at the resonance frequency ω_0; the resulting transverse component $M_\mathrm{n} \sin\theta$ rotates in the xy-plane and is detected in a receiver coil (Fig. 12.49). The magnetization along B_z has been reduced from M_n to $M_\mathrm{n} \cos\theta$. The coil for

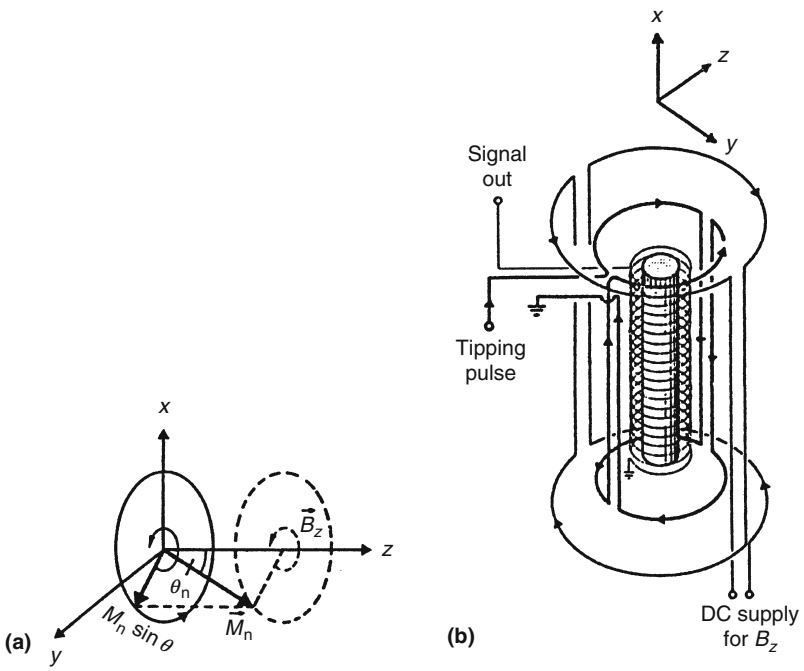

Fig. 12.49. Schematic of pulsed nuclear magnetic resonance thermometry. (**a**) Principle of the method. (**b**) Schematic of the coil arrangement [12.3,12.4,12.159,12.171]

the tipping pulse and for detection of the signal can be identical (Figs. 12.55 and 12.56) because the tipping and detection do not occur simultaneously. The precession signal in the receiver coil decays with a characteristic time given by the transverse spin–spin relaxation time τ_2 due to the dephasing of the rotating spins. An always present inhomogeneity δB_z of the static field will speed up the dephasing. The effective decay time [12.132–12.136] is then given by

$$\frac{1}{\tau_2^*} = \frac{1-P^2}{\tau_2} + \frac{\mu\mu_\mathrm{n}}{\hbar I}\delta B_z\,, \tag{12.47}$$

where P is the polarization, hence

$$M_{xy}(t) = M_\mathrm{n}(0)e^{-t/\tau_2^*}\,. \tag{12.48}$$

Such a free induction decay signal is shown in Fig. 12.50. The pulse length ($\tau_\mathrm{p} = \theta\hbar/\mu\mu_\mathrm{n}B_1$ at resonance) should, of course, be short compared to τ_2^*. This gives a lower limit on the tipping angle or on the magnitude of the pulse for a given tipping angle.

The alternating voltage induced in a detection coil in the x-direction around the sample is then given by

$$U(t) = \alpha\omega M_z \sin\theta \sin(\omega t)\exp(-t/\tau_2^*)\,, \tag{12.49}$$

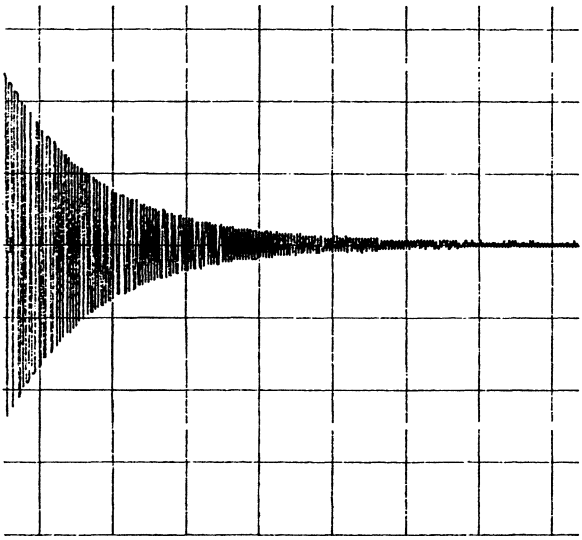

Fig. 12.50. Free precession signal of ^{195}Pt nuclear spins (2,000 wires of 25 µm diameter in a 5 mm long secondary coil of several thousand windings of 25 µm Cu wire, see Fig. 12.55) at $T = 45\,\mu\mathrm{K}$ and in $B = 13.8\,\mathrm{mT}$ (125 kHz). The excitation pulse was 64 µs long and had about $0.2\,\mathrm{V_{pp}}$ amplitude. The horizontal scale is $0.5\,\mathrm{ms\,div^{-1}}$

where α is the geometry or coil constant. This behavior can be calculated from its equation of motion (Bloch equations) [12.3,12.4,12.132–12.135,12.156, 12.157].

$U(t)$ has to be amplified and transformed into a signal S which is usually the integral over a definite time of the rectified free-induction-decay signal (Fig. 12.50). The only way to determine the constant of proportionality between S and T_{n}^{-1} is the calibration at a known higher temperature and setting the product signal * temperature constant. For this proportionality to be valid, τ_2 has to be temperature independent [12.161]. In addition, no other background contribution to the signal should be present (see below). Deviations from a linear relation between signal size and temperature can also be observed when the excitation pulse or other external RF signals will overheat the platinum NMR probe (see Fig. 12.54).

In the NMR methods discussed earlier one is determining the nuclear spin temperature T_{n} from a measurement of the nuclear susceptibility. However, by measuring the spin lattice relaxation time τ_1 and applying the Korringa law $\kappa = \tau_1 T_{\mathrm{e}}$, one can also use NMR to measure the temperature T_{e} of the electrons. This can be done by using either SQUID NMR or pulsed NMR. In the latter method one applies a 90° pulse at the resonance frequency to destroy the magnetization in the z-direction. Afterwards, small, e.g. 10°, inspection pulses are applied to record the recovery of M_z according to

$$M_z(t) = M_{\mathrm{n}}(0)(1 - e^{-t/\tau_1})\,. \tag{12.50}$$

An example of such a measurement is illustrated in Fig. 12.51. A determination of the electronic temperature from nuclear magnetic properties by

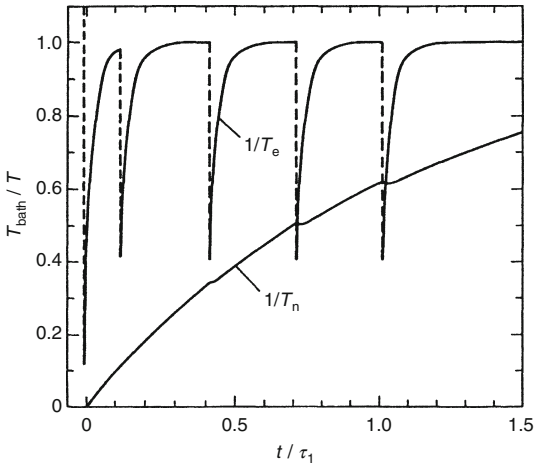

Fig. 12.51. Determination of the spin–lattice relaxation time τ_1 from pulsed NMR measurements. The figure shows the calculated time behavior of T_{n}^{-1} and T_{e}^{-1} during a τ_1 determination [12.160]

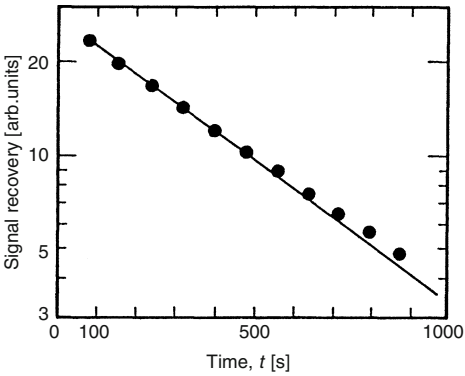

Fig. 12.52. Relaxation of the nuclear magnetization of a ^{195}Pt NMR sample after applying a 60° pulse. From the measured relaxation time τ_1 and the Korringa relation for platinum, $\tau_1 T_e = 30\,\mathrm{mK\,s}$, one finds $T_e = 61.5\,\mu\mathrm{K}$; the Pt nuclear magnetization gave $T_n = 60.5\,\mu\mathrm{K}$ [12.50]

observing the nuclear spin-lattice relaxation time τ_1 has been popular for many years [12.50, 12.157, 12.159, 12.160, 12.162]. The results of successful examples are shown in Figs. 12.52 and 12.53. However, in some experiments deviations from the Korringa law have been observed for Cu [12.163] and Pt [12.123, 12.157, 12.162, 12.164, 12.165], showing that κ can be temperature and field dependent, so that this method should only be used with great caution. These deviations have been attributed to the Kondo effect of magnetic impurities in the host lattice [12.166] but details are not yet understood.

NMR at very low temperatures is not a simple method, and the electronic setup can be quite sophisticated. However, it is the *only* method available at present for thermometry below 1 mK. There are a number of requirements which have to be fulfilled in order to obtain reliable results with pulsed NMR [12.161]. Particular care has to be taken if a large temperature range is investigated. First, we have to remember that the tipping pulse reduces the nuclear magnetization M_n to $M_n \cos\theta$; this increases the nuclear spin temperature from T_n to $T_n/\cos\theta$. For a 90° pulse this would be $M_n = 0$ and $T_n = \infty$; generally, $\Delta T/T = (\cos^{-1}\theta) - 1 (\simeq \theta^2/2$ for small $\theta)$. One has to search for a compromise between a small increase of T_n (proportional to $1/\cos\theta$) and a large enough signal (proportional to $\sin\theta$). Typically a 10° pulse is applied, giving $\cos 10° = 0.985$ or $\Delta T/T \simeq 1.5\%$ only. Calibration is always carried out at temperatures higher than the investigated temperature range and the tipping angle has to be changed to keep the signal at a reasonable level. Even more important, we have to take into account that the RF field of the tipping pulse increases the electronic temperature due to eddy current heating [12.156,12.160]. This eddy current heating is proportional to ω^2 (Sect. 10.5.2). Again a compromise between a large enough signal and small enough eddy current heating has to be found. Typical heat depositions are 0.1–1 nJ per pulse for Pt NMR

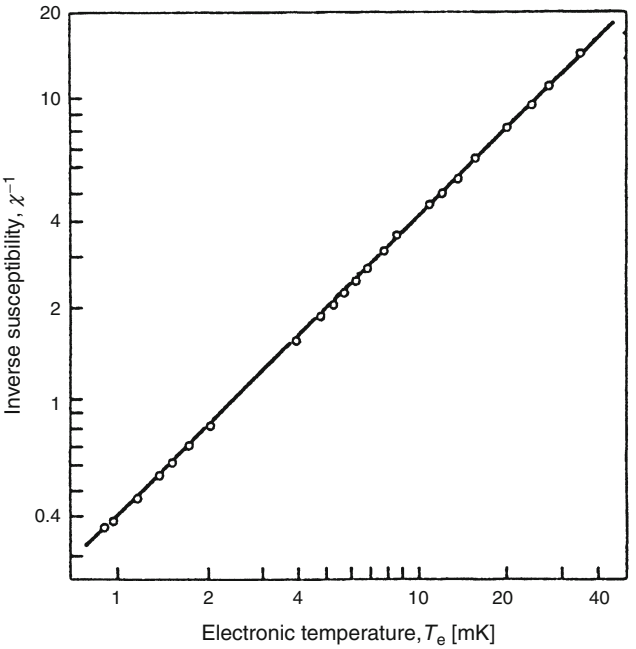

Fig. 12.53. A comparison of the reciprocal of the nuclear spin susceptibility χ_n of Pt (proportional to its nuclear spin temperature T_n) vs. the reciprocal of the spin–lattice relaxation time τ_1^{-1} of Pt (which is proportional to the shown electronic temperature T_e of Pt) to show that the nuclear spins and the conduction electrons are at the same temperature [12.172, 12.173]

thermometry at $T \leq 1\,\mathrm{mK}$ [12.50, 12.123, 12.157, 12.161, 12.167]. Overheating of the thermometer will show up if the product of the NMR signal times temperature (obtained from another thermometer) does not show a linear weak temperature dependence (Fig. 12.54).

Besides taking a low frequency and a small tipping angle, even more importantly, one has to use small dimensions of the sample, which very often means taking a bundle of thin insulated wires (or powder) for the NMR thermometry sample, to keep RF eddy current heating small and to let the electromagnetic field penetrate the sample by the skin depth $\delta = (2\rho/\mu_0\omega)^{1/2}$ which is $19\,\mu\mathrm{m}$ for high-purity Pt at a frequency of $250\,\mathrm{kHz}$. Then we have to bear in mind that after each pulse, nuclei and electrons have to recover and should be in thermal equilibrium before the next pulse is fired. Therefore the repetition rate has to be small compared to τ_1^{-1}; usual waiting times between pulses should be 5–10 times τ_1. We would also like the heat capacity of the thermometric sample (and addenda) to be small, so that we have a small thermal time constant for its thermal recovery; this means, the static field B_z should be kept as small as possible. The last requirement is in accordance with our

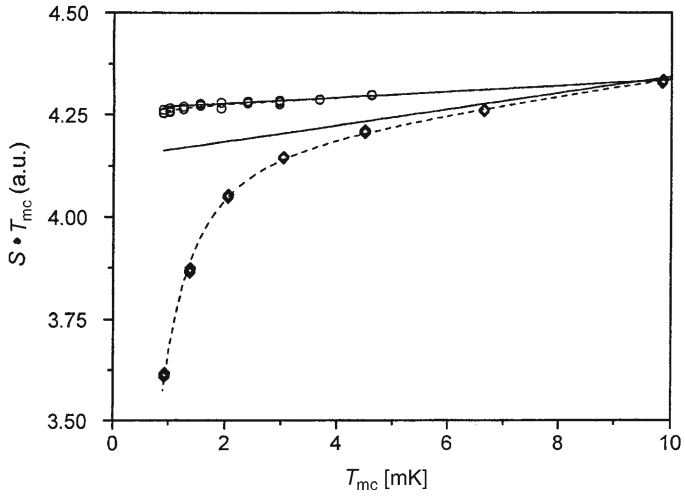

Fig. 12.54. Product of NMR amplitudes S from ^{195}Pt in Pt wire samples obtained with commercial NMR electronics times temperatures T_{mc} measured with a ^{3}He melting curve thermometer. These data show below 10 mK the overheating of the Pt wires squeezed (◇) to the cold finger of the refrigerator compared to the much better contact of wires welded to the refrigerator (○). Broken lines show the expected behavior with heating effects, full lines those without heating effects which are almost indistinguishable for the welded sample [12.161]

desire to keep the frequency for the NMR low. Last but not least, the static field should be homogeneous (to at least 10^{-4}) to give a sharp resonance and to keep τ_2^* large, see (12.47).

A main advantage of this transient method is the fact that it measures the state of the nuclear spin system before the (short!) pulse is applied and that the detection can occur when the tipping field has been switched off. The pulsed technique seems to be more appropriate for thermometry at very low temperatures than the CW method under the usual experimental conditions [12.156].

Owing to recent advances in attaining very low temperatures, one can perform experiments where the high-temperature approximations (10.4) used to describe the thermodynamic properties of a sample cannot be applied anymore. The spin dynamics can then become rather complicated because after a disturbance the nuclei will decay exponentially with a single decay time only for $I = 1/2$ [12.168–12.170]. Eventually, at $g_n\mu_n B > k_B T$, the resulting effective decay time obtained from fitting experimental data will approach a constant value, see (10.11′),

$$\tau_1 = \frac{2k_B\kappa}{g_n\mu_n B} \tag{12.51}$$

instead of being $\tau_1 = \kappa/T_e$, because now the relaxation rate depends on the magnetic rather than on the thermal energy. In this situation τ_1 decreases

with spin I according to

$$\tau_1(T=0;I) = \frac{1}{2I}\tau_1(T=0;I=1/2)\,. \tag{12.52}$$

For Cu, for example, the simple high-field limit $\tau_1 = k/T_c$ is reached for $B > 10\,\mathrm{mT}$.

In Table 10.1, I have summarized the properties of several metallic isotopes which may also be suitable for NMR. From these properties and the experience of several groups it turns out that Pt seems to be the most suitable thermometric probe at very low temperatures. It has only one isotope, ^{195}Pt, with nuclear spin $I = 1/2$; therefore we have no problems with nuclear quadrupole interaction. It has a short τ_1; this means, that electrons and nuclei quickly attain thermal equilibrium. Its nuclear spin–spin relaxation time τ_2 is long; therefore the decay of the signal takes a long time, simplifying observation of the signal.

Pulsed NMR on thin Pt wires (or Pt powder immersed in liquid ^{3}He) at fields of 6–60 mT and correspondingly at frequencies of about 55–550 kHz is now the standard thermometric method for the microkelvin temperature rangex [12.50, 12.123, 12.137, 12.158–12.161, 12.164, 12.165, 12.171–12.175]. A bundle of several hundred or, better, thousand thin (e.g., 25 μm), annealed (but see [12.123]) and isolated wires and not too high frequencies are chosen to keep eddy current heating low and to let the RF field penetrate the sample wires (the skin depth is of order 10 μm at $\nu = 250\,\mathrm{kHz}$ for Pt with RRR $\simeq 100$). Successful designs of Pt wire NMR thermometers are shown in Figs. 12.55 and 12.56 [12.50,12.123,12.161]. These thermometers have a signal-to-noise ratio of 1 at about 0.1 K. Figure 12.57 shows the calibration of a Pt wire thermometer with a *Pd*Fe susceptibility thermometer (Sect. 12.9), which in turn had been calibrated by a superconducting fixed point device (Sects. 11.4.2, 11.4.3). Such an NMR thermometer and the described calibration is believed to give the temperature at 1 mK (20 μK) to ± 2%(± 5%), assuming the fixed point device temperatures to be correct [12.50, 12.123, 12.137]. The data in Fig. 12.56 also demonstrate that $\chi_n(\mathrm{Pt}) \propto \chi_e(Pd\mathrm{Fe})$ to within 10^{-3}, or that both susceptibilities follow a Curie (or Curie–Weiss) law to that accuracy in the investigated temperature range. Usually the accuracy of an NMR thermometer is limited by the accuracy of the calibration and by heating effects [12.156, 12.161].

The validity of the ^{195}Pt NMR temperature scale has also been confirmed to at least 70 μK by the observation that $B/T_{Pt} = \text{const.}$ in the adiabatic nuclear demagnetization experiments of [12.123], and to at least 100 μK by the observation that the relative change of the velocity of sound of polycrystalline Ag is proportional to $\ln T_{Pt}$ [12.107]. In addition, in [12.50] it was shown that T_n (from χ_n) and T_e (from τ_1) agree to within 2% from 48 to 306 μK (Fig. 12.52). These as well as other observations [12.137] provide convincing evidence that the Pt-NMR temperature scale is correct to at least 10 μK. In recent experiments NMR and AC susceptibility measurements on Pt have been utilized successfully for thermometry to an equilibrium temperature of 1.5 μK

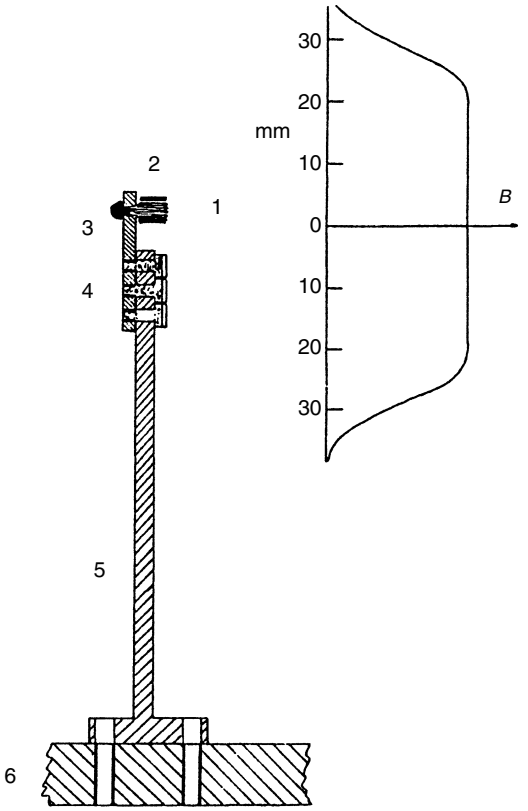

Fig. 12.55. Design of a platinum wire NMR thermometer. *Left*: Pt wires of 25 µm diameter (1) which sit inside of a signal coil of 25 µm Cu wire on a 6 µm Mylar coil former (2). The platinum wires are welded to assure adequate thermal contact into a Pt stem (3) which is then screwed (4) to a Ag cold finger which has a very small unclear heat capacity (5). The latter is finally screwed to the plate (6) whose temperature the thermometer is supposed to measure. The setup is surrounded by a coil producing the static field which is surrounded by a superconducting niobium shield to homogenize the field and to shield against external disturbances. *Right*: The field distribution of the superconducting field coil

and to a nuclear-spin temperature of 0.3 µK [12.176]. These convincing experimental observations agree with expectations because the electron-mediated indirect exchange interactions between the nuclei in platinum correspond to about 0.2 µK (this actually is a rather high value caused by the large indirect exchange interaction between the Pt nuclei due to the large polarizability of the conduction electrons in the strongly paramagnetic Pt). In addition, the Lorentz field and the demagnetization effect for a cylindrical sample transversal to the applied field are of the same order of magnitude and they partially

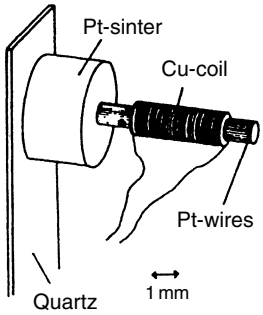

Fig. 12.56. Platinum wire NMR thermometer for measuring the temperature of liquid helium. The Pt wires (e.g., 25 μm diameter) are pressed into a platinum black sinter of 0.25 g. The latter provides a large surface area of $4\,m^2$ to make thermal contact with the liquid. It is preferable to do the NMR on the Pt wires rather than on the very fine Pt powder directly because the latter usually contains a large fraction of impurities and its NMR resonance may also be more strongly influenced by size and strain effects. The thermometer is held by a quartz sheet and a copper signal coil is wound around the Pt wires

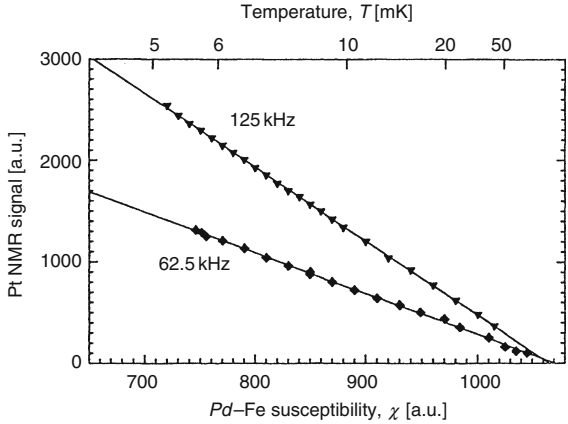

Fig. 12.57. Calibration of the NMR signal of a platinum wire NMR thermometer versus electronic paramagnetic susceptibility of *Pd*Fe (Sect. 12.9) in the temperature range between 5 and 50 mK at the two frequencies shown. The vertical scale is different for the two frequencies [12.123]

cancel each other [12.161]. Hence, the Pt NMR signal in not too high magnetic fields should be proportional to T_n^{-1} to the mentioned temperatures. However, the properties of platinum are strongly influenced by magnetic impurities [12.38, 12.161, 12.176]. For example, Fe, the most abundant magnetic impurity in Pt, forms so-called giant magnetic moments of $\mu = 7.8\ \mu_B$ at low Fe concentrations in the Pt matrix [12.38]. The main effect of magnetic impurities is a reduction of the spin-spin relaxation time $\tau_2 = 1.2$ ms of pure

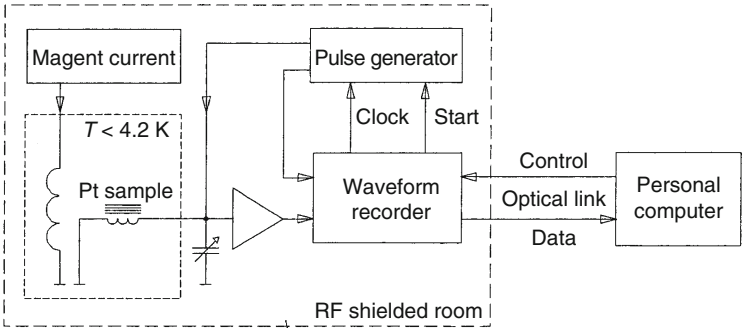

Fig. 12.58. Block diagram of the electronics used in [12.161] for pulsed NMR thermometry on ^{195}Pt. A 12-bit waveform recorder is used for signal detection. It is controlled from outside the shielded room via an IEEE bus and an optical link. The recorder actuates the pulse generator which in turn triggers the recording. A common time base ensures the coherence of individual free induction decays. The signals are averaged and analyzed in a computer

Pt to slightly temperature dependent values in the range of 0.1–0.5 ms for Pt of 4N purity, and 0.3 to 0.9 ms for 5N purity samples [12.161, 12.176]. A further reduction of τ_2 results from radiation damping, i.e., that the spins are not only influenced by the pulse field but by the induced signal as well. Above all, the inhomogeneity of the external DC field has to be less than $3\ 10^{-5}$ to keep changes of τ_2 to below 5%. Any reduction of τ_2 changes the proportionality between the free-induction-decay (FID) signal and the magnetization or temperature. The discussion of these as well as of further effects on τ_2 can be found in [12.161].

At very low temperatures, pulsed NMR on ^{195}Pt usually is performed at 250 kHz (sometimes half of this frequency) corresponding to a field of 28.4 mT. For signal recording, a pulse generator, a wide-band preamplifier, and a waveform recorder as a detector are needed (Fig. 12.58). However, because of the widespread use of pulsed Pt NMR, there is a complete electronic setup for this purpose on the market, which rectifies the FID electronically and indicates the mean value of a predefined section of it; it operates at various fixed frequencies and adjustable pulse/tipping angle strengths. For data acquisition and signal processing, i.e., analysis of signal properties, coherent background corrections, back extrapolation, as well as consistency checks (for example, how well the FID follows an exponential function; plot of NMR signal times temperature obtained from another thermometer (Fig. 12.54), etc.), the reader should consult [12.161], for example. The analysis of the various factors in this reference leads to the conclusion that for a sample as shown in Fig. 12.55, with the appropriate wiring, stable and linear electronics, signal averaging (to reduce incoherent noise and to improve the signal-to-noise ratio, which is only typically about 10 at 15 mK), and calibration (see Fig. 12.57, for example) the total uncertainty of this thermometry method can be as low

as 0.5% at 1–15 mK. The importance of these detailed investigations were necessary because pulsed nuclear magnetic resonance on ^{195}Pt and the validity of the Curie law for its nuclear magnetic susceptibility were essential in establishing the new temperature scale PLTS-2000 at $T < 15$ mK (Sect. 11.3). However, NMR on ^{195}Pt has exclusively been used up till now in all experiments for $T < 1$ mK. This indicates the urgent need for the development of alternative thermometric methods for this temperature range to substantiate the obtained temperatures. Deviations from the Curie law and time constant problems may limit the present thermometric methods to $T \gtrsim 1\,\mu$K anyway.

Even though electronic magnetic impurities have no direct influence on the signal in nuclear resonance methods, they may have an indirect influence by changing the local magnetic field seen by neighbouring host nuclei or by influencing the relaxation rate. This may have a pronounced effect on the data if the investigated temperature range includes characteristic temperatures like the Kondo temperature for Kondo alloys [12.166] or the spin-glass freezing temperature for spin glasses [12.38, 12.123, 12.161].

12.11 Magnetic Thermometry via Anisotropy of Gamma Rays (Nuclear Orientation Thermometry)

Nuclear magnetic thermometry relies on the detection of the Boltzmann population of magnetic sublevels, that is, of the nuclear magnetic polarization. The detection is via measurement of the resulting magnetization or via measurement of the change in magnetization due to resonant RF radiation (see Sect. 12.10). In this section, I will discuss another way to detect nuclear polarization which can be applied if radioactive nuclei are used. Radioactive long-lived nuclei suitable for nuclear orientation thermometry usually show a $\beta^{\pm}$-decay feeding a short-lived excited state which then decays by emission of γ-rays (Fig. 12.59). If the long-living $\beta^{\pm}$-emitters are polarized, the polarization is transferred to the excited, γ-ray emitting state. This γ-ray then has an emission probability with a spatial anisotropy that differs for each of the $(2I + 1)$ sublevels in a magnetic field. The spatial anisotropy is a result of the conservation of angular momentum. The γ-radiation field carries an angular momentum which is the difference of the angular momenta of the two nuclear sublevels involved. The angular momentum of the emitted radiation determines the multipole character of the radiation.

If we have an ensemble of radioactive nuclei, the mean value for the emission probability is equal in all directions. We have to orient the nuclei to be able to detect the spatial anisotropy of the emitted γ-ray intensity, which is a result of the Boltzmann population of the sublevels and therefore of the temperature. The anisotropy depends on the parameters of the nuclear transition and on the polarization of the nucleus. The anisotropic emission of γ-rays

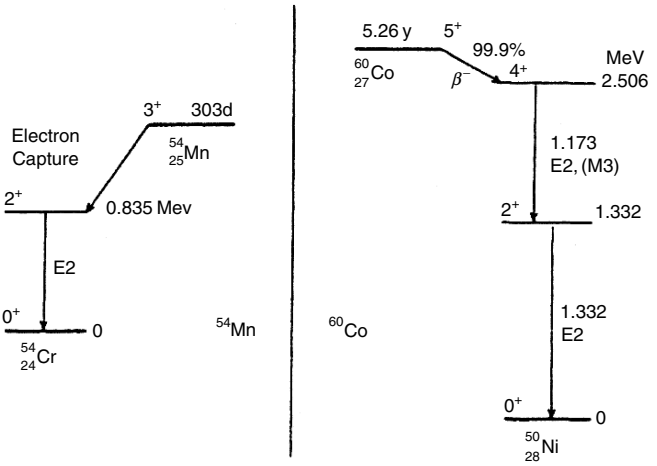

Fig. 12.59. Energy level diagrams for ^{54}Mn and ^{60}Co (slightly simplified). These are the two favorite decay schemes used for nuclear orientation thermometry

from an assembly of oriented nuclei can be used for thermometry if all other parameters determining the γ-ray intensity are known.

The intensity of the γ-radiation emitted from axially symmetric nuclei and detected at an angle θ, which is the angle between the direction of orientation of the nuclei (or of the magnetic field) and the detection or observation of the radiation, is given by [12.3, 12.4, 12.7, 12.10, 12.177–12.182]

$$W(T,\theta) = 1 + \sum_{\mathrm{k}=2,4,6,\ldots}^{\mathrm{k}_{\max}} Q_{\mathrm{k}} U_{\mathrm{k}} F_{\mathrm{k}} B_{\mathrm{k}}(T) P_{\mathrm{k}}(\cos\theta)\,; \qquad (12.53)$$

this value has been normalized to the intensity at high temperatures, where the probability is equal in all directions. In the summation we have only to consider even k-values because γ-quanta have a spin 1, and the interaction which determines the transition between two nuclear levels resulting in emission of a γ-ray is parity conserving. The parameter k will run to $k_{\max} = 2I$ or $2\,L$, whichever is smaller, where L is the multipolarity of the emitted radiation. The parameters in the above equation are:

Q_{k} Geometry parameter (detector properties, finite size of source, finite angle of detection, etc.); often the experiment can be designed so that the Q_{k}'s are of order "1", but they have to be determined for each experiment (see [12.177])

U_{k} Influence of polarization of the former nuclear transitions on the polarization to be used for thermometry; this is "algebra" and can be taken from tables in the literature [12.182, App. 5]

F_{k} Angular momentum coupling coefficients of the nuclear transition; again this can be taken from tables [12.182, App. 5]

B_k Population of nuclear magnetic sublevels [12.182, App. 6]
P_k Legendre polynomials expressing the angular dependence of the γ-ray distribution
θ Angle between γ-ray emission and axis of orientation.

The essential parameter for our thermometric purpose is

$$B_k = I^k \frac{(2k)!}{(k!)^2} \sqrt{\frac{(2I+1)(2k+1)(2I-k)!}{(2I+k+1)!}} f_k(I) \tag{12.54}$$

with

$$I^2 f_2(I) = \sum_{m=-I}^{+I} m^2 P(m) - \frac{I(I+1)}{3}, \tag{12.55}$$

and

$$I^4 f_4(I) = \sum_{m=-I}^{+I} m^4 P(m) - \frac{I^2(6I^2+6I-5) f_2}{7} - \frac{(3I^2+3I-1)I(I+1)}{15}. \tag{12.56}$$

In these equations $P(m)$ is the Boltzmann population probability of the sublevel with the magnetic quantum number m; these $P(m)$ are given in (9.9). They are the only T-dependent parameters in the above equations.

The nuclear decay level schemes of the two most commonly used isotopes, ^{60}Co and ^{54}Mn, are shown in Fig. 12.59. These two isotopes are attractive because all the necessary nuclear parameters are known, the lifetime of the intermediate state is short so that reorientation effects can be neglected, and they are pure E2 transitions giving a purely electric quadrupole radiation pattern with multipolarity $L = 2$ (2) and nuclear spin $I = 3$ (5) for ^{54}Mn (^{60}Co), therefore $k_{max} = 4$. Figure 12.60 shows the angular radiation pattern for ^{60}Co for various values of $k_B T/\Delta m g_n \mu_n B$. For the mentioned isotopes the relevant parameters are:

$$U_2F_2 = -0.49486;\ U_4F_4 = -0.44669 \text{ for } ^{54}\text{Mn},$$
$$U_2F_2 = -0.42056;\ U_4F_4 = -0.24280 \text{ for } ^{60}\text{Co},$$

$$P_2(\cos\theta) = (3\cos^2\theta - 1)/2,$$
$$P_4(\cos\theta) = (35\cos^4\theta - 30\cos^2\theta + 3)/8.$$

With these parameters we find eventually for E2 radiation detected at an angle $\theta = 0$ [12.3]

$$W(T,0) = 1 + 0.38887\ Q_2 \sum_m m^2 P(m) - 0.55553\, Q_4 \sum_m m^4 P(m)$$

for ^{54}Mn, and

$$W(T,0) = 1 + 0.04333\ Q_2 \sum_m m^2 P(m) - 0.00333\, Q_4 \sum_m m^4 P(m)$$

for ^{60}Co.

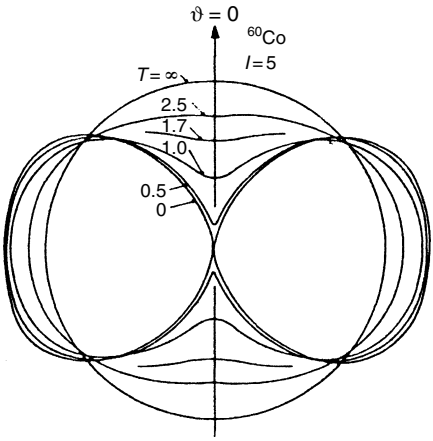

Fig. 12.60. Angular radiation pattern of ^{60}Co for several values of $k_{\mathrm{B}}T/\mu\mu_{\mathrm{B}}\mathrm{B}$. The figure demonstrates that the highest sensitivity for temperature changes is obtained when the detector is in the $\theta = 0$ or 180° directions where the maxima of the intensity change occur when the temperature is changed

In order for the nuclei to be polarized or oriented they have to experience a magnetic field. This can be an externally applied field, or as has been done in most cases, we can implant the radioactive isotope into a ferromagnetic host matrix, for example, ^{60}Co into a Co or Fe single crystal (deposit radioactive material on a host metal and then let it diffuse at high T). In this matrix the nuclei experience a large internal hyperfine field which can be of the order of 10–30 T if the isotope is implanted in a ferromagnetic 3d host. If we use this latter method we only have to apply a small field (0.1–1 T) to orient the magnetic domains for saturation of the matrix and to define a quantization axis.

The γ-ray detector should be in a direction where the change of the γ-ray intensity is a maximum as a function of temperature. As Fig. 12.60 demonstrates, this is the case for angles $\theta = 0$ or 180°, if we have an E2 transition. We have to correct for any background contributions to the radiation, for geometry effects, and for the intensity of our source by performing a measurement at high temperatures where $W(T, \theta) = 1$.

Using radioactive nuclei for thermometry one has to be careful not to produce too large a self-heating of the source due to radioactive transitions. Typical values are for

1 μCi^{60}Co : 0.57 nW due to the β-emission,
and
1 μCi^{54}Mn : 0.03 nW due to the 5 keV radiation from radioactive ^{54}Cr after electron capture; [12.3, 12.4, 12.7, 12.10, 12.21, 12.177–12.182].

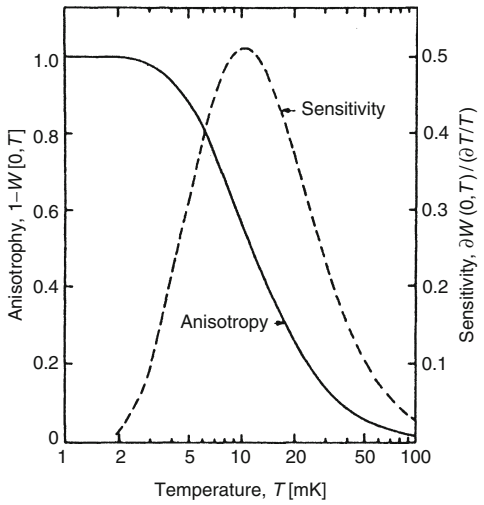

Fig. 12.61. Temperature dependence of the anisotropy of the γ-radiation of ^{54}Mn in an Ni host along $\theta = 0$. The quantity $\mathrm{d}W/\mathrm{d}T$ is a measure of the temperature sensitivity of the thermometer which, in this case, has its maximum value at about 10 mK

In an appropriate experimental setup the high-energy γ-rays used for thermometry can leave the source without noticeable heating effects. If the source is too strong it will heat; if it is too weak, counting times may get excessive. In any case the source has to be in good thermal contact to its surrounding. This can usually even be achieved by soldering because the polarizing field will keep the solder normal-conducting.

One of the disadvantages of nuclear orientation thermometry is that the sensitivity $T(\mathrm{d}W/\mathrm{d}T)$ is limited to a certain temperature range at around a value of $T \cong \Delta m \mu_\mathrm{n} g_\mathrm{n} B/k_\mathrm{B}$, which is usually between 1 and 100 mK (Fig. 12.61). For the earlier mentioned isotopes we have $\Delta E_\mathrm{m}/\mathrm{k_B} = 9.14\,\mathrm{mK}$ for ^{54}Mn in Fe and 7.97 mK for ^{60}Co in Fe (corresponding to internal fields of $-22.7\mathrm{and}-29.0\,\mathrm{T}$, respectively). Therefore for these transitions the useful range is a few millikelvin to about 40 mK, whereas at higher and lower temperatures $W(T, \theta)$ is independent of T because all levels are either equally populated or only the lowest level is populated.

Because this method is a statistical method we need a certain counting time to obtain the desired accuracy. The error of the measurement due to statistics is $\Delta T/T = (2/n)^{1/2}$ if we count n pulses. One typically needs a measuring time of several minutes to half an hour to get an accuracy of 1%, for example, because the source must not be too strong in order to avoid self-heating. Low-temperature physicists sometimes unjustifiably avoid this method because they do not have the counting and detecting electronics on hand, which is more common in nuclear physics laboratories (the basic equipment consists of a γ-ray detector, like GeLi, a preamplifier, gate, and a multichannel analyser with a computer).

An advantage of this method is that we can use a metal to make good thermal contact to the point whose temperature we want to measure and to have a good nuclear spin–lattice coupling. The γ-energy is very often large enough that we do not need special windows to get the γ-rays out of the cryostat. We do not need any leads to the sample because we only measure the electromagnetic field of the γ-rays. And, finally, nuclear orientation is a primary thermometric method because the theory is well established, and we do not need any extra calibration except that we have to normalize the counting rate or the intensity of the radioactive source at high temperatures. Therefore this method has very often been applied for calibration purposes [12.10, 12.21, 12.172, 12.173, 12.182, 12.183].

Detailed and instructive comparisons between various nuclear orientation and other thermometric methods are described in [12.177–12.183]. In some of these papers as well as in other relevant work discrepancies observed between the various temperature scales were reported, with many of them originating from self-heating effects or from incomplete magnetic saturation (aligning of domains) of the γ-ray source; in some cases fields in excess of even 1 T seem to be necessary for complete magnetization. Some of the observed discrepancies are not yet fully understood. Agreement to better than 0.5% at 10–50 mK has been found in [12.183] for a Josephson noise thermometer and a ^{60}Co γ-ray anisotropy thermometer. The main usefulness of a γ-ray anisotropy thermometer may remain as a primary thermometer for calibration purposes in a restricted temperature range and for nuclei with well-understood decay schemes. For example, nuclear orientation of the γ-rays emitted from ^{60}Co has been used as the primary thermometric method at 0.5–25 mK in the contribution of the University of Florida [12.21] to the realization of the new temperature scale PLTS-2000 (see Sect. 11.3).

Another method relying on the Boltzmann population of nuclear sublevels of radioactive nuclei is the Mössbauer effect. This method has not often been applied and, for more details, the literature cited in [12.3, 12.4] should be consulted. A disadvantage of it is that one can only use low-energy γ-rays ($E \leq 100$ keV) requiring in most cases special thin windows to let the γ-rays escape from the cryostat. In addition, corrections for finite sample thickness, long counting times, specialized equipment and motion of source or absorber are necessary.

12.12 Summary

Table 12.3 summarizes the most important thermometric methods for determination of temperatures below 1 K. They are resistance measurements on a conductor of $T > 20$ mK and susceptibility measurements of the electronic paramagnetism for the temperature range above a few millikelvin. Below this temperature one has to resort to nuclear magnetism where the nuclear susceptibility in most cases is measured either directly or more appropriately

Table 12.3. The most commonly used thermometric techniques at $T \leq 1\,\mathrm{K}$

Measured property	Function	Material	Temperature range
Electrical resistance	$\ell \mathrm{n} R = \sum_{\mathrm{n}=0}^{\mathrm{m}} \alpha_{\mathrm{n}} (\ln T)^{\mathrm{n}}$	Composites with negative R–T characteristics	$> 20\,\mathrm{mK}$
Electronic param. suscept.	$\chi_{\mathrm{e}} = \chi_0 + \lambda_{\mathrm{e}}/(T_{\mathrm{e}} - \Delta)$	CMN; PdFe	$> 3\,\mathrm{mK}$
Nuclear paramag. suscept.	$\chi_{\mathrm{n}} = \chi_0 + \lambda_{\mathrm{n}}/\mathrm{T_n}$	Pt	$1\,\mu\mathrm{K}$–$0.1\,\mathrm{K}$

via one of the discussed nuclear magnetic resonance methods. Here one relies on the applicability of the Curie law. The result of each temperature measurement has an error and it deviates more or less from the absolute thermodynamic temperature. Very often it is difficult to estimate the uncertainty of the measured "temperature". In cases where temperature is a very important parameter, such as in measurements of heat capacities, it is sometimes advisable to use two different thermometric methods and compare the results if possible to get a feeling for the uncertainty in T. In any case, it is very important to write up the obtained results with all relevant experimental details so that future researchers can reconstruct the used temperature scale, and, if necessary, later corrections are possible. A low-temperature physicist should always remember that the quality of his data depends on the quality of his thermometry!

Problems

12.1. Which voltage resolution is necessary to measure with a (Au + 2.1% Co vs. Cu) thermocouple a temperature of 30 mK to about 1% (Fig. 12.4)?

12.2. Which relative voltage resolution is necessary to measure 20 K with a platinum resistance thermometer to 1%?

12.3. Suppose a carbon thermometer of $5\,\mathrm{mm}^2$ area is immersed in liquid helium at 1 K and the Kapitza resistivity is $\mathrm{AR_K}T^3 = 0.01\,\mathrm{K}^4\,\mathrm{m}^2\,\mathrm{W}^{-1}$. What is the maximum dissipation allowed in the resistor for a temperature difference of $\Delta T = 0.1\,\mathrm{mK}$ between it and the liquid-helium bath?

12.4. Calculate the thermal response time of a Speer 220 Ω thermometer at about 1 K. Take for the heat capacity typical values shown in Fig. 12.16 and for the thermal resistance the value given in the middle of p. 294.

12.5. Calculate the relative sensivity of the thick-film chip-resistors for which the equation and characteristics are given in (12.10) and Fig. 12.22.

12.6. Deduce (12.13) and (12.14) from (12.12).

12.7. Which sensitivity of a voltmeter is necessary to measure via noise thermometry 1 K to 1% at a bandwidth of 1 MHz using a resistor of 100 kΩ?

12.8. Calculate the relative sensitivity to which the capacitance of the capacitive glass thermometer, whose behavior is exhibited in Fig. 12.35, has to be measured to determine a temperature of 10 mK to 1%.

12.9. Calculate how many ppm of Fe impurities (magnetic moment $\mu = 2\,\mu B$) would give the same electronic susceptibility as its host Cu would contribute nuclear susceptibility.

12.10. At which temperature does the nuclear Curie law deviate by more than 1% from the exact solution (9.15c) for the magnetization of a platinum NMR thermometer used in 25 mT (Fig. 10.5)?